DOKUZ EYLÜL UNIVERSITY

GRADUATE SCHOOL OF NATURAL AND APPLIED SCIENCES

SYNTHESIS OF NANOMATERIALS AND INVESTIGATION OF THEIR SENSING PROPERTIES ALONG WITH $[Ru(bpy)_3]^{2+}$ COMPLEX

by

Elif MUSLU

January, 2020

İZMİR

SYNTHESIS OF NANOMATERIALS AND INVESTIGATION OF THEIR SENSING PROPERTIES ALONG WITH $[Ru(bpy)_3]^{2+}$ COMPLEX

A Thesis Submitted to the
Graduate School of Natural and Applied Sciences of Dokuz Eylül University in Partial Fulfillment of the Requirements for the Degree of Master of Science in Nanoscience and Nanoengineering Program

by
Elif MUSLU

January, 2020
İZMİR

M.Sc THESIS EXAMINATION RESULT FORM

We have read the thesis entitled **"SYNTHESIS OF NANOMATERIALS AND INVESTIGATION OF THEIR SENSING PROPERTIES ALONG WITH $[Ru(bpy)_3]^{2+}$ COMPLEX"** completed by **ELİF MUSLU** under supervision of **PROF. DR. ELİF SUBAŞI** and we certify that in our opinion it is fully adequate, in scope and in quality, as a thesis for the degree of Master of Science.

Prof. Dr. Elif SUBAŞI

Supervisor

Doç. Dr. Nur AKSUNER

(Jury Member)

Prof. Dr. Kadriye Ertekin

(Jury Member)

Prof. Dr. Kadriye ERTEKİN
Director
Graduate School of Natural and Applied Sciences

ACKNOWLEDGMENTS

First of all, I would like to point out my deepest appreciativeness to my supervisor Prof. Dr. Elif SUBAŞI for their endless support, advice, and patience.

Who lent her academic guidance throughout all experience and help during my thesis work, Prof. Dr. Kadriye ERTEKİN. It was a pleasure to study with her and to have a chance to benefit from her scientific and personal experience for her leading throughout all experiments.

I also thankfully acknowledge that funding was procured by the Scientific and Technological Research Council of Turkey (TUBITAK) (1002 Short term R&D Funding Program, project number: 218Z026).

Finally, I would like to thank my family, especially to my mother Kevser MUSLU and my father Salih MUSLU for their sustained supports and tolerant attitudes to my working effort during enhancement of this thesis and for understanding during all the times of my studies.

Elif MUSLU

SYNTHESIS OF NANOMATERIALS AND INVESTIGATION OF THEIR SENSING PROPERTIES ALONG WITH $[Ru(bpy)_3]^{2+}$ COMPLEX

ABSTRACT

In this study, optical properties of tris(2,2-bipyridyl)ruthenium (II) chloride ($[Ru(bpy)_3]^{2+}$), a ruthenium complex, together with various nanoparticles (TiO_2 and core-shell TiO_2@Ag nanoparticles) were investigated in the oxygen-permeable polymeric material. Plasticizer containing polymethylmethacrylate (PMMA) was shaped in form of thin film by applying the spin coating process and its optical properties and sensitivity towards oxygen were observed. It is known from previous studies that the $[Ru(bpy)_3]^{2+}$ complex exhibits extraordinary optical properties and high oxygen sensitivity when embedded in the above-mentioned matrix and used in combination with silver nanoparticles. In our thesis, the presented design is totally different from the earlier published literature. The porous and straight thin composite films were fabricated via the spin coating technique. Unlike the previous studies, the semiconductor TiO_2 and core-shell TiO_2@Ag nanoparticles were doped into these composite materials and the spectral properties of the prepared thin films were examined. Luminescence signal variations resulting from the application of oxygen sensor at 626 nm were recorded.

Keywords: Ruthenium complex, TiO_2 and core-shell TiO_2@Ag nanoparticles, thin film, spin coating technique, oxygen sensor

NANOMALZEMELERİN SENTEZİ VE $[Ru(bpy)_3]^{2+}$ KOMPLEKSİ İLE BİRLİKTE SENSÖR ÖZELLİKLERİNİN ARAŞTIRILMASI

ÖZ

Bu çalışmada, bir rutenyum kompleks olan tris(2,2-bipyridyl)ruthenium(II) chloride ($[Ru(bpy)_3]^{2+}$) 'nin optik özellikleri, çeşitli nanoparçacıklarla (TiO_2 ve çekirdek-kabuk TiO_2@Ag nanoparçacıklar) birlikte oksijen geçirgen polimerik materyal içerisinde incelenmiştir. Plastikleştirici içeren polimetilmetakrilat (PMMA), spin kaplama tekniği uygulanarak ince film kompozit malzeme haline getirilmiş, optik özellikleri ve oksijene karşı duyarlılığı incelenmiştir. $[Ru(bpy)_3]^{2+}$ kompleksinin yukarıda belirtilen matrise gömüldüğünde mükemmel optik özellikler ve yüksek oksijen duyarlılığı sergilediği ve gümüş nanoparçacıklarla birlikte kullanıldığında ise oksijene karşı duyarlılığında daha iyi verim alındığı önceki çalışmalardan bilinmektedir. Yaptığımız tez çalışmasında bu kompleksin oksijen algılama mekanizması, daha önceki yayınlanmış bu tür çalışmalardan çok farklı gerçekleşmiştir. Gözenekli ve pürüzsüz ince kompozit filmler spin kaplama tekniği ile elde edilip, daha önceki çalışmalardan farklı olarak yarıiletken TiO_2 ve çekirdek-kabuk TiO_2@Ag nanoparçacıklar bu kompozit malzemelerin içerisine doplanmış, hazırlanan ince filmlerin spektral özellikleri incelenmiştir. 626 nm'de oksijen sensör uygulaması sonucu oluşan luminesans sinyallerindeki değişiklikler kaydedilmiştir.

Anahtar kelimeler: Rutenyum kompleks, TiO_2 ve çekirdek-kabuk TiO_2@Ag nanoparçacıklar, ince film, spin kaplama tekniği, oksijen sensör

CONTENTS

Page

LIST OF FIGURES

Page

LIST OF TABLES

Page

CHAPTER ONE
INTRODUCTION

Oxygen plays an essential character in human life and numerous biological processes, chemical and biochemical reactions (Choi & Xiao, 1999). And so, exact measurement of oxygen concentration is terrific interest in diverse fields such as biology, agriculture, medicine, and the food sector. In addition, such importance of oxygen measurement in the industrial dimension can be comprehended providing that every car has an oxygen sensor.

Nowadays, electrochemical and optical sensor strategies are widely used in gas or dissolved oxygen detection. Clark electrodes, a sort of electrochemical oxygen sensor, are broadly used measuring mechanism in prior studies (Clark, 1956). Such electrodes work with respect to the change in electric current in feedback to the oxygen reduction reaction (Clark, 1956). However, the oxygen sensation which uses the Clark electrode reduces the amount of oxygen during measurements, is restricted spot analysis of the sample area, and can not exactly diagram the oxygen distribution (Wang & Wolfbeis, 2014; Wolfbeis, 2015).

The other side, oxygen sensors which have optical properties do not run out of oxygen and may notice the concentration of oxygen on a surface area that allows accurate and real-time oxygen detection (Choi & Xiao, 1999; Wang & Wolfbeis, 2014; Wolfbeis, 2015). Besides, such sensors offer indispensable advantageous features such as faster response, exact detection, outstanding sensitivity, reversibility, cost efficient, simple reproducibility and the possibility of miniaturization (Mills, 1997; Wu et. al., 2018; Kurihara, Ikegami, Asahi, & Tanabe, 2018).

In this study, optically functional ruthenium molecules were used as sensing material in selected polymeric matrix and after doping of different nanoparticles suitable for this complex, composite materials were fabricated by spin coating technique. Sensor applications of the produced membranes were examined. Luminescence based measurements mainly were performed. Therefore, a short explanation regarding to the terminogly of the luminescence is given below.

1.1 Definition and Theory of the Luminescence

The term luminescence is described as the emission of light after exposure of the complexes to the stimulus source. Diverse sorts of luminescence can be listed as, chemiluminescence, crystalloluminescence, electroluminescence, mechanoluminescence, radioluminescence, thermoluminescence, and photoluminescence named according to the source from which energy is attained (Lakowicz, 1993; Parker, 1968; Schmidt, 1994; Yamamoto, 2003) (See Table 1.1).

Table 1.1 Sort of luminescence and its corresponding mechanisms

Types of Luminescence	Mechanism
Chemiluminescence	Chemical reaction
Bioluminescence	Biochemical reaction by a living organism
Electrochemiluminescence	Electrochemical reaction
Crystalloluminescence	Crystallization
Electroluminescence	Electric current passed through a substance
Cathodoluminescence	Struck by electrons
Mechanoluminescence	Mechanical action on a solid
Triboluminescence	Bonds in a material are broken
Fractoluminescence,	Bonds in certain crystals are broken by fractures
Piezoluminescence	Action of pressure on certain solids
Sonoluminescence	Imploding bubbles in a liquid when excited by sound
Photoluminescence	Absorption of photons
Fluorescence	Singlet–singlet electronic relaxation
Phosphorescence	Triplet–singlet electronic relaxation
Radioluminescence	Bombardment by ionizing radiation
Thermoluminescence	Re-emission of absorbed energy when a substance is heated

1.1.1 Chemoluminescence

Chemoluminescence is the emission of light, in consequence of a chemical reaction and the direct output of the reaction is an excited electronic state. An electronic ground is decayed into state and transmitted light through both an allowed and a forbidden transitions, depending on the spin state of the electronically excited state formed (Vacher et al., 2018).

Such luminescence is different from types of photoluminescence (fluorescence

and phosphorescence). The electronic excited state is the product of a chemical reaction instead of the photon absorption. It is the opposite of a photochemical reaction utilized light energy to drive chemical reaction which spends energy. Shortly, light is created from a chemically reaction (Vacher et al., 2018).

1.1.2 Crystalloluminescence

The effect of luminescence generated throughout crystallization is clarified crystal luminescence or crystalloluminescence. The appearances were first inscribed in the 1800s from the fast crystallization of potassium sulfate from an aqueous solution (Zink & Chandra, 1982).

1.1.3 Electroluminescence

Electroluminescence has both optical and electrical aspect. In this process, the material can give out light when an electric current or an intense electric field passes over. In addition to this, if the material is a semiconductor such as metal oxides, it can emit light due to radiative recombination of the electron-hole dual of which. The excited electrons deliver their energy as photons light (Zhang & Roosmalen, 2009). In case of inorganic materials like metal oxides or phosphors before recombination, electron-hole dual can be distributed by doping the material to set off a p-n junction (light-emitting diodes, (LEDs)). Another factor that occurs the electroluminescence is that excitation owing to the influence of electrons possessing high energy stimulated by a strong electric field (such as phosphor). For example, the solar cell operates according to the electroluminescence principle, and it has been emphasized in these studies that the use of electricity is efficient as well as developing the open-circuit voltage (Raguse & Sites, 2015).

1.1.4 Mechanoluminescence

Mechanoluminescence is light emission resulting from any mechanical operation, for example, tribological, fractal, and compressional deformation (though piezo) on solid material can be produced.

1.1.5 Radioluminescence

Alpha, beta and gamma beams which is ionizing radiation bombard material thereby, it product illumination. Such an operation is called radioluminescence. The luminescence might be used as night vision of devices, machines or materials. It can be also seen around high-power radiation sources, such as nuclear reactors and radioisotopes (Murthy & Virk, 2014).

1.1.6 Thermoluminescence

Thermoluminescence is one of the luminescence classes that is exhibited by some minerals such as crystalline material. The material heated that is why absorbs energy and afterwards, the material re emit as illumination as long as heating (Bos, 2006).

1.1.7 Photoluminescence

Photoluminescence is described as the re-emission of a photon from a material when a photon is absorbed by the material. Depending upon the re-emission of the photon, it is again distinguished into two types: fluorescence and phosphorescence. Figure 1.1 points out a Perrin-Jablonski diagram showing fluorescence and phosphorescence (Yamamoto, 2003).

The Perrin–Jablonski diagram emphasizes complete possible processes regarding luminescence which are photon absorption, internal conversion, fluorescence, intersystem crossing, phosphorescence, delayed fluorescence and triplet-triplet transitions (See Figure 1.1). The singlet electronic states referred as S_0 (ground electronic state), S_1 or S_2 (excited electronic states); and the T_1, T_2…T_n (triplet states). Vibrational energy levels are connected with each electronic state. Luminescence process initiate with excitation where the light energy is absorbed by the atom or molecule. Among the above-mentioned processes, absorption is the fastest process ($1x10^{-15}$s) with respect to all other transitions (Lakowicz, 1993; Parker, 1968; Schmidt, 1994).

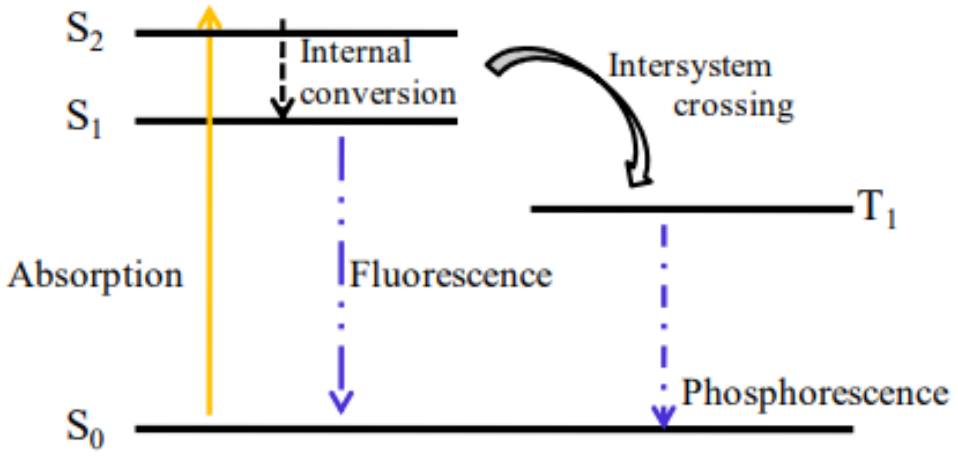

Figure 1.1 The Perrin–Jablonski illustration (Yamamoto, 2003)

Many of molecules are at the lowest level; S_0 at room temperature, therefore the absorption starts from the S_0 vibrational level. Absorption of a photon is probable to induce the transition of electrons to one of the upper vibrational levels of S_1, S_2… (Lakowicz, 1993; Parker, 1968; Schmidt, 1994).

Internal conversion is a co-energetic radiationless transition between two electronic states of the equal diversity in a compound or atom. It is called "radiationless deactivation" because no photons are emitted. The energy of the electronically excited state is given off to vibrational levels of the atom or molecule or to the micro environment of the emitting species. In the absence of the radiation he excitation energy is generally transmuted into heat (Bancroft, Moore, & Frazier, 1976) (See Figure 1.1).

1.1.7.1 Fluorescence

Some atoms and molecules absorb light at a particular wavelength. Later, they emit usually at less energy which has a little time slot, which is named the fluorescence lifetime. Emission of photons from the lowest vibrational level of the excited S_1 to ground S_0 relaxation is named fluorescence. The lifetime of an excited singlet layer is almost between the approximately 10^{-8} seconds. If fluorescence is not undisturbed by other challenging processes, the lifetime of fluorescence is the characteristic speciality of the excited singlet state. Forbye, fluorescence might be measured for both transparent and opaque sections (Yamamoto, 2003).

1.1.7.2 Intersystem Crossing

Intersystem crossing is a nonradiative manner taking place between two co-energetic vibrational levels possession to unlike multiplicities (Bancroft vd., 1976). Intersystem Crossing may come about in the time interval of 10^{-7}–10^{-9} s challenging with other paths of fluorescence.

1.1.7.3 Phosphorescence

In most of the photoluminescence, an atom or a molecule absorbs and then re-emits a light, which ensue at a level of 10 nanoseconds. When the photons energy content matches the available energy states and allowed transitions light is absorbed and emitted at such a little time intervals.

Nevertheless, in the event of phosphorescence, the energy of the absorbed photon undergoes an intersystem crossing into an energy state of higher spin multiplicity which is generally a triplet state This energy trapped in the triplet is generally returned to the lower energy state with only "forbidden" transitions. Since these transitions are "forbidden", they are kinetically unflavored and occur at substantially slower time intervals. Phosphorescent materials exhibit generally lifetimes arising from triplet transitions on the order of milliseconds. However, some complexes exhibit triplet lifetimes extending to minutes or even hours. Figure 1.2 brings to light the simple paths of phosphorescence.

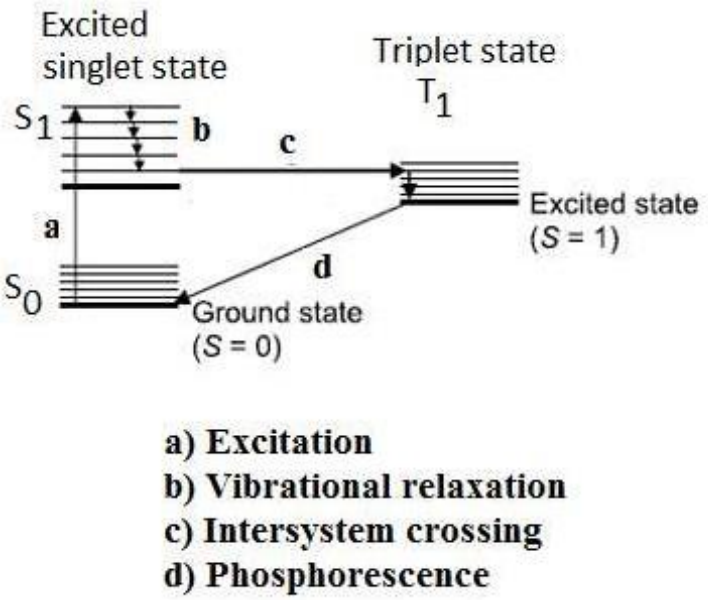

Figure 1.2 Simple transition eventuating in course of the phosphorescence

1.1.7.4 Stoke's Shift

Stoke's shift is defined as the alteration amongst the peak maximum of the absorption and emission spectra of the associated electronic conversion. The large Stoke's shift of the well-known luminescence material. Shortly, the difference in energy or wavelength between excitation and emission photon is called the Stoke's shift (See Figure 1.3).

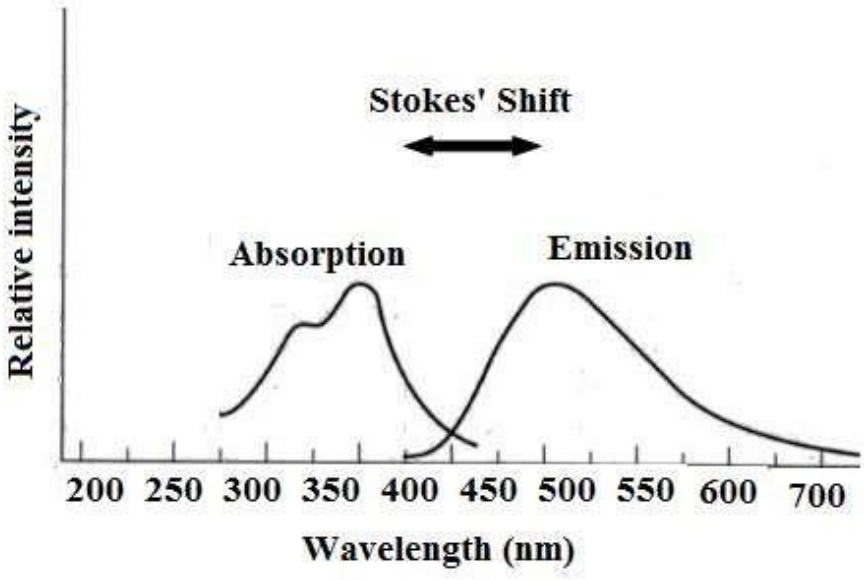

Figure 1.3 Representation of the absorption and emission spectra and Stokes shift

1.2 Quenching Mechanism for Oxygen Sensor Applications

Quenching occurs by different mechanisms like excited state reactions, molecular rearrangements, energy transfer, ground-state complex formation, and collisional quenching. The luminescence quenching phenomenon seen in luminescence-based optical oxygen sensors can be defined as a decrease in luminescence density of luminophore, which have luminescence properties. There are two types of quenching principle, static and dynamic luminescence quenching, and optical oxygen sensors are mainly based on the dynamic quenching principle (collisional quenching).

Papkovsky, 2004 describes luminescence quenching with the oxygen molecule in the following diagram:

$$D + h_{1/2} \longrightarrow D^{*} - excitation$$
$$D^{*} \xrightarrow{k_L} D + h_{1/2} - emission$$
$$D^{*} + O_2 \xrightarrow{k_Q} D + O_2{}^{*} \equiv collisional\ quenching, no\ emission \quad (1.1)$$

In this scheme, D and D* represent the ground and excited state of the luminophore, respectively; O and O* represent the ground and excited states of the oxygen molecule. k_L and k_Q coefficients are luminescence and quenching ratio coefficients, respectively.

The frequency phase of the collisions between oxygen and luminophore molecules is called dynamic luminescence quenching and might vary depending on the concentration, pressure and temperature of the oxygen.

In the oxygen sensor, the relationship between intensity and O_2 concentration is expressed by the Stern-Volmer equation. The Stern-Volmer constant (K_{sv}) measures the efficiency of the quenching and is described as the sensitivity of the sensor.

$$I_0 / I = \tau_0 / \tau = 1 + Ksv\ [O_2] \quad (1.2)$$

I_0 and I represent luminescence intensities in the absence and presence of oxygen while τ_0 and τ indicate the decay time of the luminophore in so on, respectively. In the case of dynamic quenching, when the oxygen concentration increases, the luminophore's emissivity intensity and lifetime decreases. The graph drawing should be linear and equivalent according to the oxygen concentration I_0 / I and τ_0 / τ for such quenching. In short, the oxygen sensing complex is excited and then emits light where the intensity, decay time or wavelength depends on the oxygen concentration (Papkovsky, 2004).

1.3 Lifetime

Lifetime (τ) is one of the most significant features of luminescent material and generates time available for the material to interact with exciting photons or diffuse the photons in its environment. When a specimen is excited with a light, an initial population (n_0) of it is in an excited state. For a two level system i.e., ground state and exited state, the population of the excitation state decays with a rate $\Gamma + k_{nr}$ according to

$$dn(t) / dt = - (\Gamma + k_{nr}) n(t) \qquad (1.3)$$

where n(t) is the number of excited molecules at time t following the excitation pulse; Γ is radiative decay and k_{nr} is non-radiative decay to the ground state (Blasse, Grabmaier, Blasse, & Grabmaier, 1994; Lakowicz, 2003; Yamamoto, 2003). Emission is a random process and each excited molecule or ion has the same probability of emission in a given interval of time. This outcomes in an exponential decay of the excited state population,

$$n_{(t)} = n_0 \exp(-t/\tau) \qquad (1.4)$$

where $\tau = 1/(\Gamma + k_{nr})$ is the lifetime of the specimen. The number of excited molecule or ion, n(t), is not observed in photoluminescence experiment, but photoluminescence intensity, I(t), is observed. The two are related as $I(t) \propto - dn(t) / dt$. Thus, the above equation is be written in terms of time dependent intensity, I(t) as:

$$I_{(t)} = I_0 \exp(-t/\tau) \quad (1.5)$$

where I_0 is the intensity at time 0. Hence, the photoluminescence lifetime can be determined from the plot of log I(t) vs. t while the emission of light is a random process and few molecules/ions emit photons at precisely $t = \tau$. After a time τ the population of the excited state has decreased to 1/e (37%) and the rest (63%) have decayed prior to $t = \tau$. Actually, the decay time is also defined as the time for the intensity to drop by 1/e or to 37% of the τ (Yamamoto, 2003).

The average lifetime <t> for bi-exponential decay is:

$$\langle t \rangle = (I_1 \tau_1^2 + I_2 \tau_2^2) / (I_1 \tau_1 + I_2 \tau_2) \quad (1.6)$$

where $I = I_1 \exp\{-(t/\tau_1)\} + I_2 \exp\{-(t/\tau_2)$, is the bi-exponential decay law; I_1 and I_2 are intensities at two different values of time (t), τ_1 and τ_2 (Yamamoto, 2003).

1.4 Various Complexes and Ruthenium Complexes for Oxygen Sensing

In the earlier studies, many complexes such as organic or inorganic have been exploited in optical oxygen sensors (Demas, DeGraff, & Coleman, 1999; Amao, 2003; Xue, Behera, Xu, Viapiano, & Lannutti, 2014). These complexes; polycyclic aromatic hydrocarbons (Papkovsky, 2004), pyrene and its derivatives (Ishiji & Kaneko, 1995; Demas et al., 1999; Wang et al., 2010), pyrene butyric acid (Ishiji & Kaneko, 1995), transition metal complexes, osmium (Xu, Kneas, Demas, & DeGraff, 1996; Papkovsky, 2004) , rhenium (Yoshihara, Hirakawa, Hosaka, Nangaku, & Tobita, 2017), platinum (Wu et al., 2010; Mao et al., 2018) palladium (Papkovsky, 2004; Chu & Chuang, 2014) iridium (Toro et al., 2010; Maia et al., 2018), rhodium (Borisov & Vasil, 2004) and ruthenium (Choi & Xiao, 1999; Jiang, Yu, Zhai, & Hao, 2017), (Kurihara et al., 2018; Bruner et al., 2014; Miller, 2011), polypyridine complexes and metalloporphyrins (Gulino et al., 2006; de Acha et al., 2017). Various structures composed of carbon atoms such as fullerene (buckyballs) have also been nominated as oxygen sensors, radiation characteristics and oxygen sensing applications have been look overed (Amao, 2003; Wang ., 2010).

Most optical oxygen sensors using organic complexes have a short shelf life and

sometimes degrade by leaching in aqueous environments. Covalent bonding of such complexes to the matrice may abolish leaching, nevertheless the sensor's facility of the complex may be reduced (Wang et al., 2010; Aydın, 2017). Furthermore, most of these organic complexes do not have luminescence at room temperature. Therefore, complexes that can be quenching are limited (Amao, 2003).

Wu et al. (2018), unlike organic complexes of inorganic perovskite nanocrystals $CsPbA_3$ (A = chlorine, bromene or iodine) narrow size distribution, narrow absorption bands combined with large absorptions, short radiation life, color adjustment and simple synthesis processes have been informed that due to these properties, they have made studies in the field of oxygen sensor. To improve their stability by using crosslinkers in polymeric matrices such as PMMA and PS, these nanocrystals have been immobilized and prepared micro-patterned sensors with the interactive peraltion of polymeric material chemistry and micro or nano printing techiniques. Film quality and oxygen sensitivity are expressed in I_0 / I_{100} that I_0 is the luminescence intensity under nitrogen and I_{100} is the luminescence intensity under oxygen. They found that micro material impressed the sensibility feature and response time of the sensors, but observed that the quality of the films produced when cross-linking was used excessively and the oxygen permeability decreased. Besides, based on the information obtained in their research, they found that sensitivity and response time was less and slower than previous sensors (Wu et al., 2018).

In recognition of optical oxygen sensors applications ruthenium complexes are the most preferred complexes account of their longevity and strong luminescence properties. For example, Ruthenium (II) complexes and derivatives are the most commonly used complexes in the application of optic oxygen sensors owing to their ability to efficiently quench the oxygen molecule, high photo compatibility, fast response time and high sensitivity (Choi & Xiao, 1999; Zhang, Lei, Mai, & Liu, 2011; Jiang et al., 2017; Kurihara et al., 2018).

Amao reported that the transition metals are the most widely used Rudpp complexes among the polypyridyl complexes in oxygen sensor applications (Amao, 2003).

Wang et al. (2010), remarks that even though ruthenium (II) polypyridyl molecules are commonly used in oxygen sensor applications, their sence impretion in complex based oxygen sensors are not sufficiently high due to their relatively short life and singlet oxygen formation which is destructive to organisms and their use is limited only in low oxygen conditions such as space research (Wang et al., 2010).

Ongun et al. (2013) were used the fluorescent $[Ru(bpy)_3]^{+2}$ complex in polymeric electrospun mats for the detection of oxygen and the offered composite materials provided high sensitivity for oxygen and unusual long term stability (Ongun, Oter, Sabanci, Ertekin, & Celik, 2013).

Ruthenium metalloporphyrins are also among the most frequently used complexes for luminescence-based oxygen sensor applications (de Acha et al., 2017). Nevertheless, they demonstrate significant photobleaching rates when exposed to continuous illumination. Yoshiara and co-workers, declared that metalloporphyrins perform only in measurements of low oxygen concentrations, even though they have an extremely high lifetime (Yoshihara et al., 2017).

However, the $[Ru(bpy)_3]^{+2}$ complexes are still most intensively used oxygen indicators in embedded in polymeric matrices. In this work, we used the $[Ru(bpy)_3]^{+2}$ complex along with nano-scale TiO_2 and TiO_2@Ag core-shell structures in plasticized PMMA matrix. We produced the sensing slides by using Spin Coating Device on Mylar support. Response of the $[Ru(bpy)_3]^{+2}$ complexes towards oxygen is well known. However, herein we investigated effect of the optically active nano-scale TiO_2 and TiO_2@Ag core-shell structures on the oxygen sensitivity of the ruthenium complex by introducing different concentrations of oxygen. Only the TiO_2@Ag core-shell structure enhanced the oxygen induced sensitivity of the ruthenium complexes.

CHAPTER TWO
EXPERIMENTAL METHOD AND INSTRUMENTATION

2.1 Reagents

All of the materials exploited were analytic rank and purchased from Fluka, Merck, Sigma Aldrich, and Tinsa Gas. The plasticizer that is dioctyl phthalate (DOP) was procured from Fluka. The ionic liquid (RTIL), 1-butyl-3-methylimidazolium tetrafluoroborate ([BMIM][BF4]), ethanol (EtOH), silvernitrate (99% of purity $AgNO_3$) and sodium borohydride (99% of purity $NaBH_4$) for core-shell nanoparticles synthesis, and Tetrahydrofuran (THF) was from Merck. The ruthenium complex, tris(2,2-bipyridyl)ruthenium(II) chloride ($[Ru(bpy)_3]^{2+}$), oxygen-permeable polymeric matrix Polymethyl methacrylate (PMMA), perfluoro-compound (PFC), nonadecafluorodecanoic acid, and titanium tetra-isopropoxide (TTIP, $Ti[OCH(CH_3)_2]_4$ were purchased from Sigma Aldrich. Oxygen and nitrogen gases tubes were of 99.99% of purity and attained from Tinsa Gas, Izmir, Turkey. All of the testing were performed at ambient temperature; approx. 25 °C.

2.1 Ruthenium Complex Tris(2,2-bipyridyl)ruthenium(II) chloride

Ruthenium complexes are unique organometallic compounds with a wide range of uses. These complexes are promising materials in many research areas such as light emitting diodes, electroluminescence devices, dye sensitive solar cells and solar energy conversion due to their suitable photophysical, photochemical and electrochemical properties, long luminescence lifetime, and large Stokes Shift. Furthermore, the Ru(II) complexes containing polypridyl and bipyridine ligands have interesting properties including strong absorption of light from the visible region by metal-ligand charge transfer (MLTC), and their exited states have relatively long lifetime due to forbidden transition from triplet excited to singlet ground state (Ocakoglu, Okur, Aydin, & Emen, 2016; Elsayed, Gaml, & Nasher, 2018).

Tris(bipyridine)ruthenium(II) chloride for using thin film production is the chloride salt coordination complex with the formula $[Ru(bpy)_3]^{2+}$ and is indicated the chemical formula and the State diagram in Figure 2.1 and 2.2, respectively.

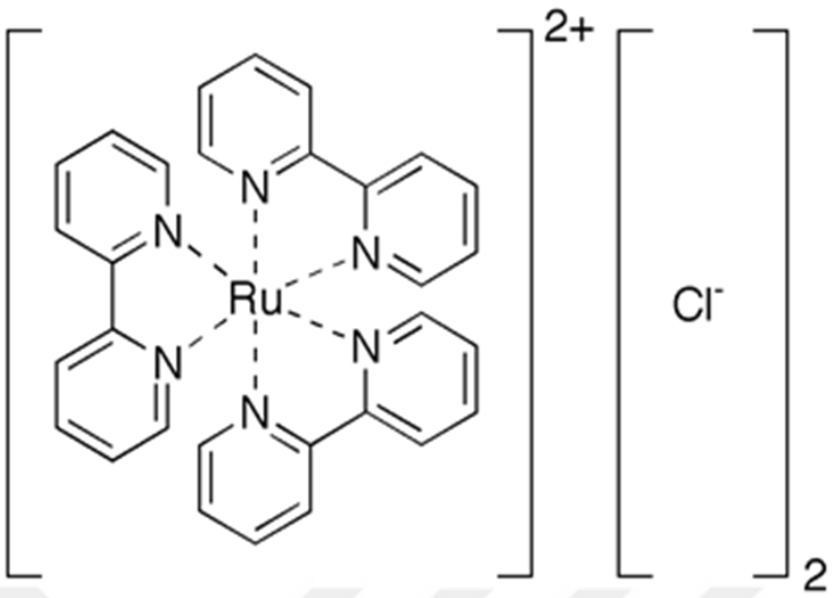

Figure 2.1 Tris(bipyridine)ruthenium(II) chloride

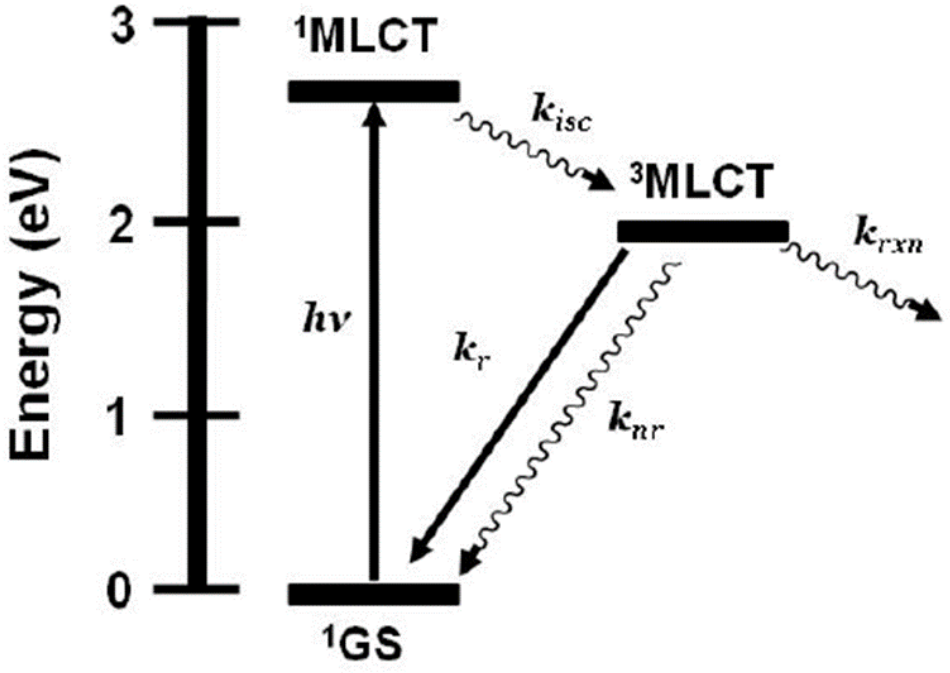

Figure 2.2 State diagram for $[Ru(bpy)_3]^{2+}$ (bpy = 2,2'-bipyridine). GS = ground state, MLCT = metal-to-ligand charge transfer excited state, kisc = intersystem crossing rate constant, kr = radiative decay rate constant, knr = non-radiative decay rate constant, krxn = photochemical reaction rate constant (White, Arachchige, Sedai, & Brewer, 2010)

2.2 Selection of Suitable Polymer for Oxygen Permeable Matrix

Matrices in which various inorganic, organic and organometallic complexes which are optically functional are doped or embedded, play a vital role in optic sensor behavior based on the luminescence quenching principle (Franciscato et al., 2018).

In case of oxygen sensors, the ideal polymer for the matrix material should exhibit high oxygen penetrability, mechanical support, chemical stability and good solubility properties for many optically functional and oxygen-sensitive complexes in order to prevent agglomeration. Highly gas-permeable polymers offer easy access to the oxygen entering the matrix, and homogeneously dispersed sensors can give responsive and linear replies to infusing oxygen molecules (de Acha et al., 2017).

To date, numerous matrice materials such as Silicon (Wu et al., 2018), PMMA (Jiang et al., 2017; S. Wu et al., 2018), EC (Tian et al., 2010; Cui et al., 2015), sol-gel (Chu & Lo, 2011) have been used. Nonlinear calibration curves for silicon-based sensors are frequently observed while sol-gel matrix optical oxygen sensors posed some problems such as nonlinear Stern-Volmer plots and pore collapse or contraction of these sensors over time (Demas et al., 1999; Xue et al., 2014). In light of this information, PMMA polymer was chosen as matrix material (See Figure 2.3).

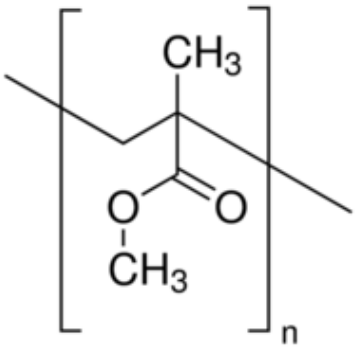

Figure 2.3 Polymethyl methacrylate (PMMA)

2.1 Nanomaterials Utilized as Thin Composite Film Additives

It is known that the optically functional ruthenium (Ru) complexes play an important role in the optical sensor behavior relaying on the luminescence quenching principle. On the other hand, the noble metal nanoparticles (gold, silver, etc.) are of interest because of their unique properties, including extensive optical field enhancements that result in strong emission and absorption of light. Recent studies have shown that the presence of conductive noble nano-sized metals such as gold and silver along with Ru complexes is effective on the optical properties of such complexes and that the strong plasmon resonance property increases the luminescence intensity (Jain, Huang, I. H. El-Sayed, & M. A. El-Sayed, 2009; Wang & Wolfbeis, 2014).

Gryczynski et al. (2003), investigated spectral properties of the $[Ru(bpy)_3]^{2+}$ complex on metallic silver particles. They observed that the relative densities on the surface containing silver particles were several times higher and the decay times were several times lower. Thus, they suggested the use of silver particles for further detectability of emission from transition metal-ligand complexes (Gryczynski, Malicka, Holder, DiCesare, & Lakowicz, 2003).

Kandimalla addressed that gold and silver nanoparticles (Ag NPs) thanks to surface plasmon resonance created a great interest and the oscillation plasmon frequency for such noble metal nanoparticles was in the visible region with strong plasmon resonance thereby, investigated the effect of three types of Ru complexes on fluorescence properties. As a result of the study, among these three complexes, the $[Ru(bpy)_3^{2+}]$ was observed to have a significant increase in the fluorescence intensity and fluorescence lifetime due to gold and silver nanoparticles and these enhanced intensities which originated in energy transfer processes from the complex to the metal nanoparticles (Kandimalla, 2010).

In another study, Jiang and co-workers embedded silver nanoparticles in a nanoporous polymeric matrix to regulate the properties of the $(Ru(DPP)_3Cl_2)$ complex. Presence of the Ag NPs resulted with enhanced Stern-Volmer coefficients (K_{sv}) good stability, response time and photostability. Nevertheless, for the Ag NPs-

doped sensor, the calibration curve became linear, and the response ranges developed for 0-15 mg / L. This is due to the spectral results taking into account the function of the Ru complex which exposed to the absorption properties of Ag NPs and the electronic transition of a metal-ligand charge transfer (MLCT) (Jiang et al., 2017).

In this thesis, TiO_2 semiconductor and TiO_2@Ag core-shell nanoparticles were used as additives and evaluated in the thin composite film for oxygen sensing application.

2.3.1 Production of TiO_2 Nanoparticles

Among the semiconductor nanoparticles, titanium dioxide nanoparticles (TiO_2 NPs) has attracted plentiful interests because of its tremendous physicochemical properties, such as proper band position, non-toxic particles, low cost, chemical and photonic stability, and biocompatibility. Moreover, it is chemically inert, stable toward corrosion and photo corrosion. In addition, such NPs is apply as food colour additives and flavour enhancers and in many cosmetics owing to their capability to absorbs and scatters ultraviolet (UV) light (Sivaranjani & Philominathan, 2016).

Generally, sol-gel nanoparticles synthesis method addressed on the conversion of subtitle procedure from a liquid “sol” (colloidal solid-liquid heterogenic solution of particles) into a gelatinous cobweb “gel” phase. This technique is a long-established industrialized method that is very cost-effective and flexible (Daraio & Jin, 2012; Dhand et al., 2015).

The sol-gel process has been used for the fabrication of ceramics, monolithic glasses, submicron particles, and aerogel materials, at a relatively low temperature. Nowadays, the process has also been used to synthesize nanoparticles in colloidal and film form. In acid solution, the transition from solution to gel form allows the solid stage to be given shape into films, fibres and monoliths. Gel fibers are made by fiber drawing from the viscous alkoxide solution at or near ambient temperature. The flow graphic representation of sol-gel processing is schematically illustrated in Figure 2.4.

In contrast to, a colloidal solution is generated upon basic hydrolysis of metal

alkoxides. The gel formulas are colloidal when the solid cobweb is made up of round sol particles (Brinker & Scherer, 2013; de Jonghe & Rahaman, 2003; Schmidt, 2010; Delice, 2018).

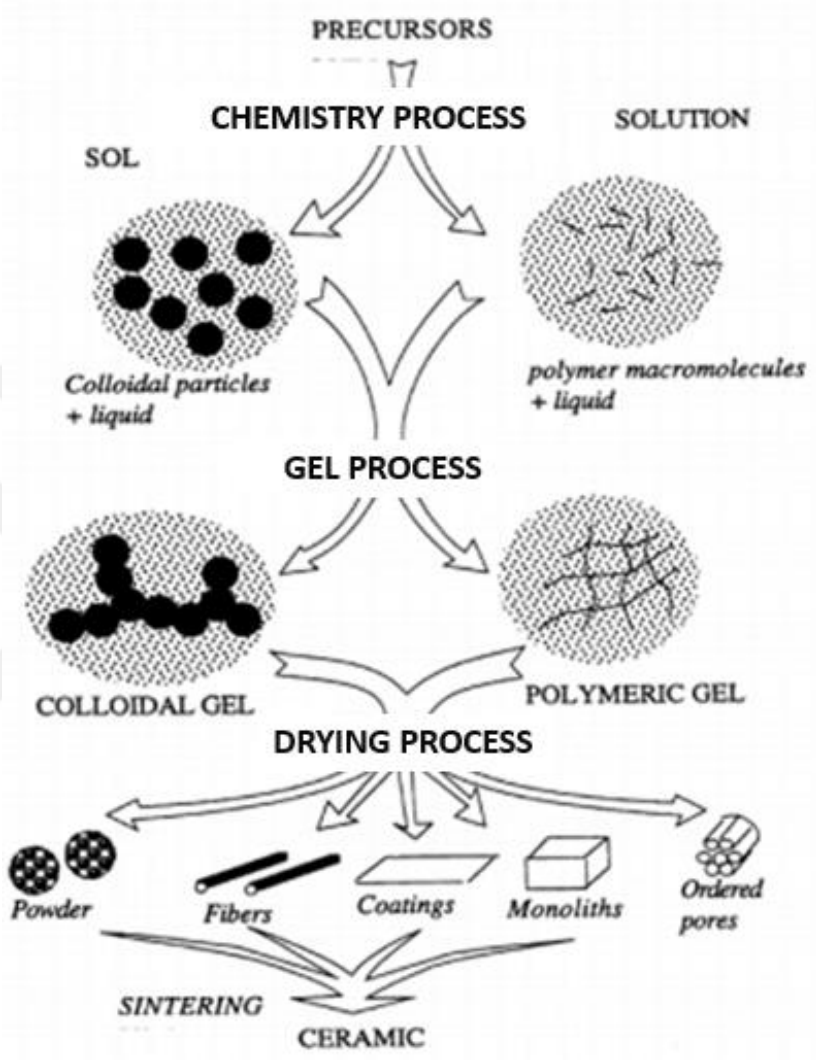

Figure 2.4 Schematic exemplification of sol-gel technique (Brinker & Scherer, 2013; de Jonghe & Rahaman, 2003; Schmidt, 2010; Delice, 2018)

The sol-gel process was utilized for the synthesis of the TiO_2 nanoparticles. 10 mL of titanium tetra-isopropoxide (TTIP, $Ti[OCH(CH_3)_2]_4$, precursor and 40 mL of ethanol (EtOH), solvent are mixed in a magnetic stirrer in the room temperature to to prepare a homogeneous solution. The resulting sol is placed on the hot plate set at 30 ºC for drying for approximately 3 hours. Following this step, it is calcined to obtain TiO_2 nanoparticles in the furnace at 450 ºC for 1 hour. The precursor and solvent used for TiO_2 nanoparticles have been shown in Figure 2.5.

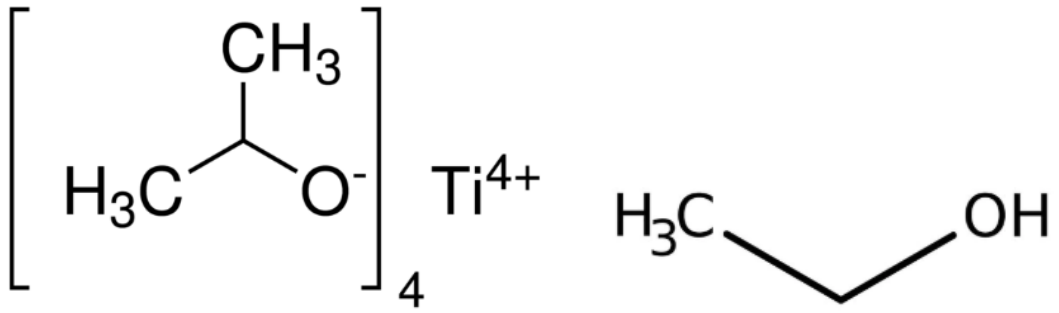

Figure 2.5 The precursor and solvent used for TiO_2 nanoparticles synthesis (left: precursor right: solvent)

2.3.1.1 Characterization of TiO_2 Nanoparticles

Phase alignment and crystal structure characteristics of the synthesized TiO_2 nanoparticles were analyzed by X-ray Diffractometer (XRD). The XRD arrays correspond to TiO_2 nanoparticles with a crystal tetragonal structure without any impurity. The XRD data of the produced TiO_2 powder was shown in Figure 2.7. It was clearly seen that the TiO_2 powder exhibits anatase phase (See Fig 2.6) (Keskin, Dalmis, Birlik, & Azem, 2020). For this nanoparticles, the (101), (004), (200), (105), (211), and (204) planes were well indexed to tetragonal TiO_2 (JCPDS 01-073-1764).

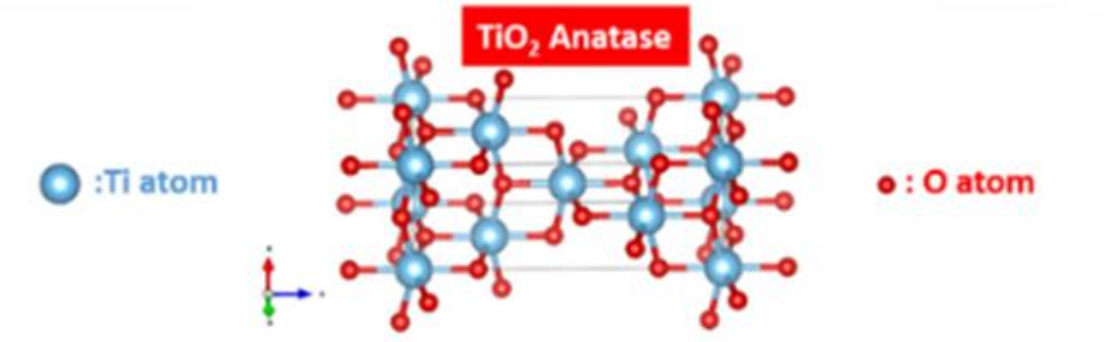

Figure 2.6 Anatase phase of the synthesized TiO_2 nanoparticles (Keskin, Dalmis, Birlik, & Azem, 2020)

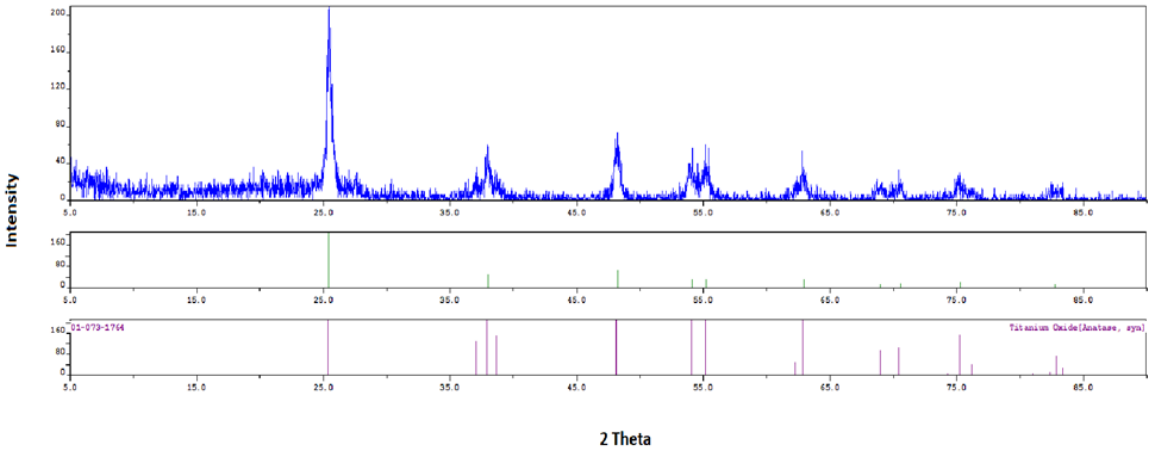

Figure 2.7 The XRD data of the synthesized TiO_2 nanoparticles

2.3.2 Production of TiO_2@ Ag Core-Shell Nanoparticles

Core@shell nanoparticles are increasingly interesting more and more attention because of the application of chemistry and many other fields, such as electronics, biomedical, pharmaceutical, optics, and catalysis and the hybrid nanomaterials are showed core/shell, core-shell, and core@shell (Ghosh Chaudhuri & Paria, 2012; Khatami, Alijani, & Sharifi, 2018).

Such nanoparticles are a type of diphase materials which have a core made of a material coated with another material on top of it (See Figure 2.8). These particles have been of interest as they can exhibit unique properties arising from the combination of core and shell material, geometry, and design. Additionally, they have been designed so that the shell material can improve the reactivity, thermal stability, or oxidative stability of the core material and these materials are also important from an economic point of view. Precious material can be coated over an inexpensive material to reduce the consumption of the precious material compared with making the same sized pure material (Nomoev et al., 2015).

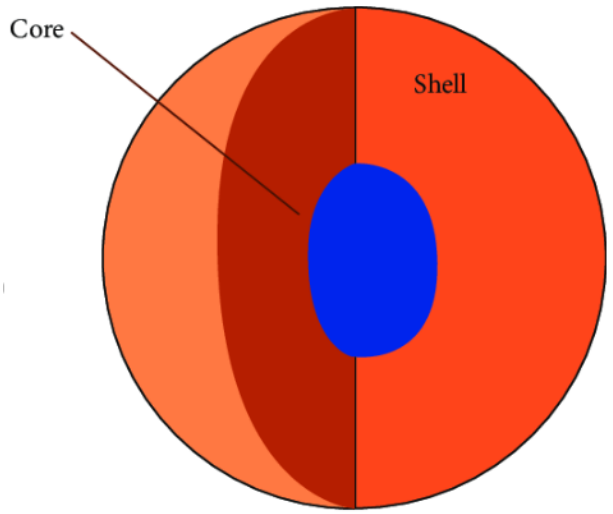

Figure 2.8 Representative structure of core@shell nanoparticles

The shell should not only nontoxic layer but also can improve properties of the core material. For example, if the core material is a semiconductor nanoparticle, the shell enhances the optical features and photostability of the core. Eventually, the nanoparticles show distinctive characteristics of the different materials when used together.

TiO_2@Ag core-shell structures have been synthesized by chemical reduction approaches. Preparation of the TiO_2@Ag core-shell forms has been performed by the reduction of the Ag^+ by using excess amount of sodiumborohydride ($NaBH_4^-$) in an ice bath under magnetic stirrer.

2.3.2.1 Characterization of TiO_2@Ag core-shell nanoparticles

Phase alignment and crystal structure characteristics of the produced TiO_2 @Ag core-shell nanoparticles were analyzed by XRD. The XRD data correspond to the core-shell nanoparticles with a crystal face centered cubic (fcc) structure without any impurity. The XRD data of the produced TiO_2@Ag powders were shown in Figure 2.9. For this nanoparticles, the (111), (200), and (220) planes were well indexed to fcc Ag (JCPDS 01-071-3762).

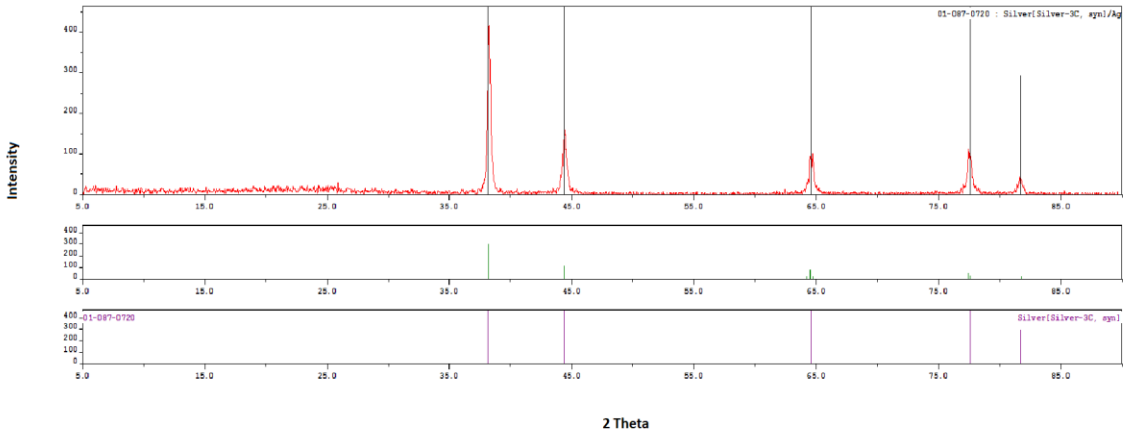

Figure 2.9 The XRD data of the synthesized TiO_2@Ag core-shell nanoparticles

2.2 Preparation of Thin Composite Films

Oxygen sensor composite materials were operated as cocktails in 5 mL of glass vials. Compositions of the utilized sensing agents were indicated in Table 2.1. In order to offer the greatest improvement in the signal intensity and to avoid the self-quenching effect, the amount of the synthesized various nanoparticles were upgraded. Polymethyl methacrylate (PMMA), plasticizer DOP, perfluorochemical, ionic liquid, several nanoparticles such as TiO_2 and TiO_2@Ag core-shell, and the organometallic $Ru[(bpy)_3]^{2+}$ molecules were dissolved in tetrahydrofuran (THF). The sensing agents of the used the chemicals were indicated in the Figure 2.10.

The compositions were mixed under the magnetic stirrer device to offer a homogeneous form at room temperature. The composites were coated onto a 125 μm polyester support (Mylar TM type) by Spin Coating Technique.

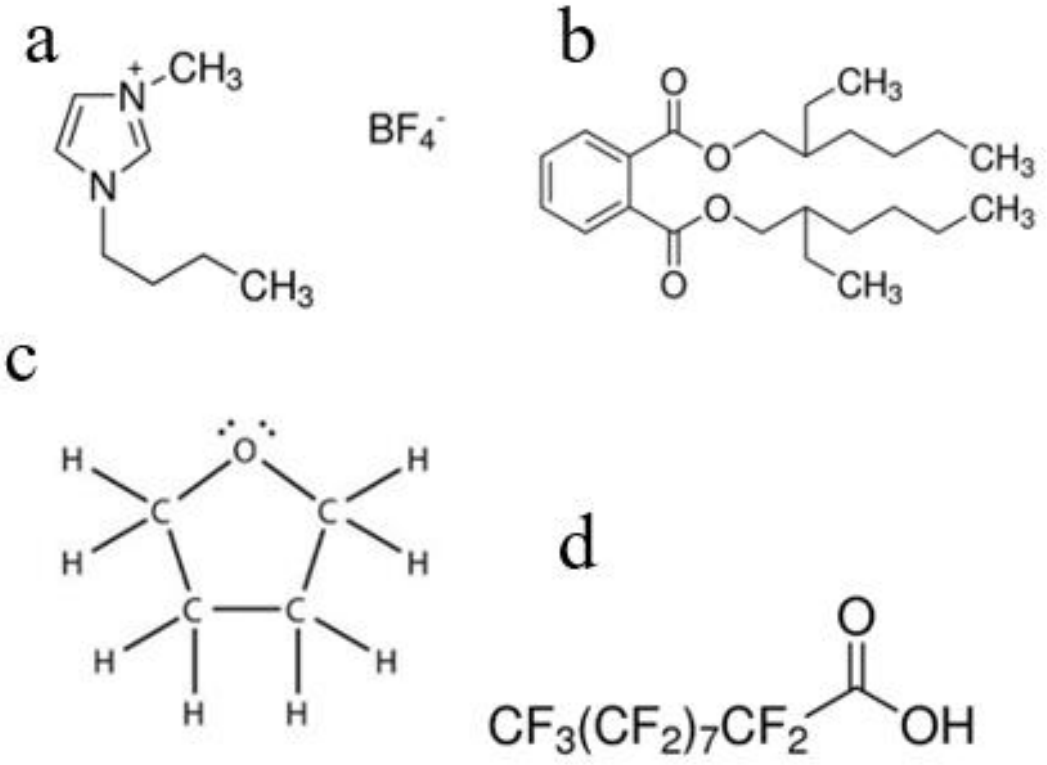

Figure 2.10 The sensing agents of the used chemicals (a ionic liquid; b DOP; c THF; d perfluorochemical)

Table 2.1 Compositions of the exploited sensing agents

Sample	Complex 1 mg	Nano Additive 1 mg	Ionic Liquid 48 mg	DOP 240 mg	Perflorodo decanoic acid 5 mg	Matrix 120 mg	Solvent 2 mL
$Ru[(bpy)_3]^{2+}$	$Ru[(bpy)_3]^{2+}$	-	+	+	+	PMMA	THF
$Ru[(bpy)_3]^{2+} + TiO_2@Ag$	$Ru[(bpy)_3]^{2+}$	$TiO_2@Ag$	+	+	+	PMMA	THF
$[Ru(bpy)_3]^{2+} + TiO_2$	$Ru[(bpy)_3]^{2+}$	TiO_2	+	+	+	PMMA	THF

2.5 Instruments

2.5.1 Spectrophotometer and Spectrofluorometer Apparatus

The fluorescence analysis of the thin composite films as used sensor application were recorded by utilized time-resolved fluorescence spectrometer of Edinburg Instruments of FLS920 which drives on the principle of time-correlated single-photon counting (TCSPC) method in steady state mode (see Figure 2.11). The specimens were excited with a microsecond flash lamp. The excitation and emission slits were tune to 10-10 nm during analysis. The Instrument Response Function (IRF) was obtained from a non-fluorescent solid-liquid heterogenic mixture of colloidal silica (LUDOX 30%, Sigma Aldrich) in water, held in 10 mm path length quartz cell and was measured to be regardless of wavelength . The diminished chi-square results and plots of weighted 27 residuals were applied to determine the 'goodness of fit' between the calculated and measured decay curves. In all cases, the calculated chi-square values ($\chi 2$) were less than 1.2 and the residuals trace symmetrically distributed around the zero axes.

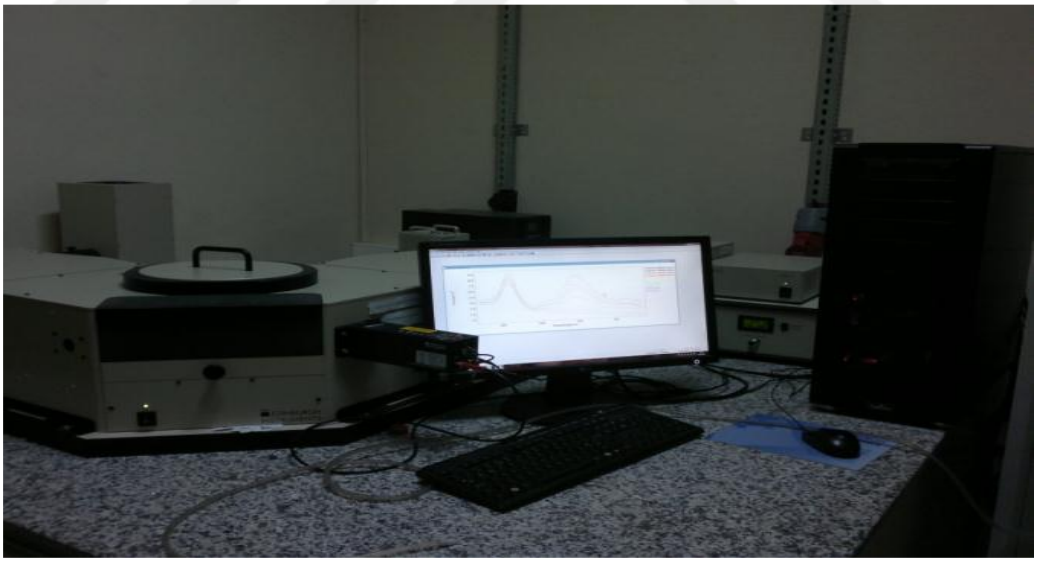

Figure 2.11 Time resolved fluorescence spectrometer (Personal archive, 2019)

2.5.2 Gas Blender

O_2 and N_2 gaseous were mixed in the concentration interval of 0–100% in a gas diluter (Sonimix 7000A gas blending system) (See Figure 2.12). The overall pressure was sustained at 760 Torr (1 Torr = 133.322 Pa). The output flow rate of the gas

mixture was maintained at 550 mL.min^{-1}. Gas mixtures were insert in the sensing material comprising cuvette via a diffuser needle under room temperature situations.

Figure 2.12 Gas blender instrument and oxygen and nitrogen cylinders (Personal archive, 2019)

2.5.3 Spin Coating Device

Spin coating method is mutual used for production thin composite film on a base. This process starts with the mixing of the material to be deposited in a solvent. The mixture is then dispensed on the base surface. Afterwards, the wafer is spun at a high speed. Figure 2.13 shows the working principles of the process. Film thickness is determined by the spinning speed, surface tension, and viscosity of the solution. The solvent is removed partly during the spin method owing to evaporation and fairly by enough baking at accerated temperatures. The spin coating results in a relatively planar surface (Microtechnologies, 2005).

The obtained viscous mixture was casted on PMMA or 125 μm Mylar (TM type) substrate by a spin-coating instrument. The device demonstrated in figure 2.14 was used to produce thin composite films. Thickness of the films was evaluated applying Ambios Technology XP-2 Surface Profilometer and were found to be 5 ± 0.1 μm.

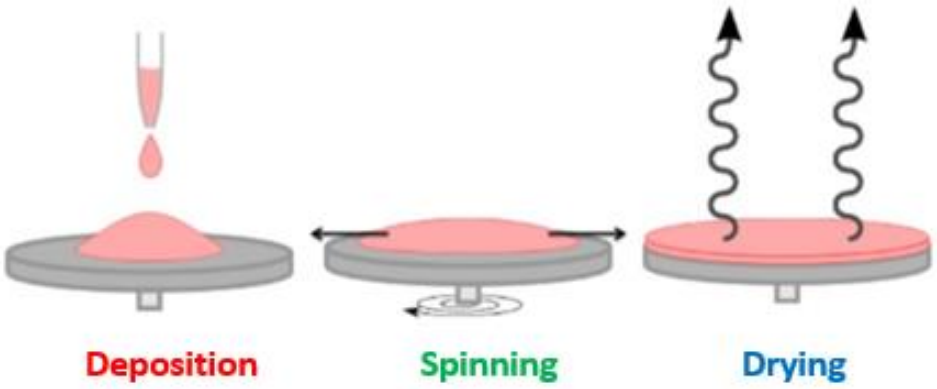

Figure 2.13 Working principles of the spin coating technique

Figure 2.14 Spin coating device (Personal archive, 2019)

2.5.4 X-Ray Diffractometer (XRD)

X-ray diffraction (XRD) is a versatile, nondestructive characterization system used to determine atomic and molecular structure of a material; size, stress measurement, etc. and operates on the attitude of diffraction.

X ray diffraction patterns of the fabricated TiO_2 and TiO_2@Ag core-shell nanoparticles were determined with this instrument from Thermo-Scientific. The XRD patterns were recorded from 30 to 90° at a speed of 2°/min.

CHAPTER THREE
OXYGEN SENSING ANALYSIS

3.1 Spectral Characterization of Thin Composite Films

3.1.1 Excitation and Emission Spectra Characteristic Analysis

We obtained fluorescence intensity, lifetime and kinetic based data following the signal of the ruthenium complex in the polymeric matrix PMMA, in presence and absence of semiconductor TiO_2 or core-shell TiO_2@Ag nanoparticles. Figure 3.1 indicates gathered excitation emission spectra of the $[Ru(bpy)_3]^{2+}$+TiO_2 based composites and $[Ru(bpy)_3]^{2+}$+TiO_2@Ag based structures, respectively. All of the utilized forms exhibit overlapped excitation and emission spectra. The TiO_2 doped ruthenium complex exhibited the lowest signal intensities pertaining to the individual ruthenium and $[Ru(bpy)_3]^{2+}$+TiO_2@Ag forms which can be attributed to the potential competition upon excitation between the TiO_2 nanoparticles and the ruthenium complex. However, the silver coated core-shell structures enhances both the emission and excitation of the ruthenium when embedded in close proximity to allow interactions between these two luminescent particles.

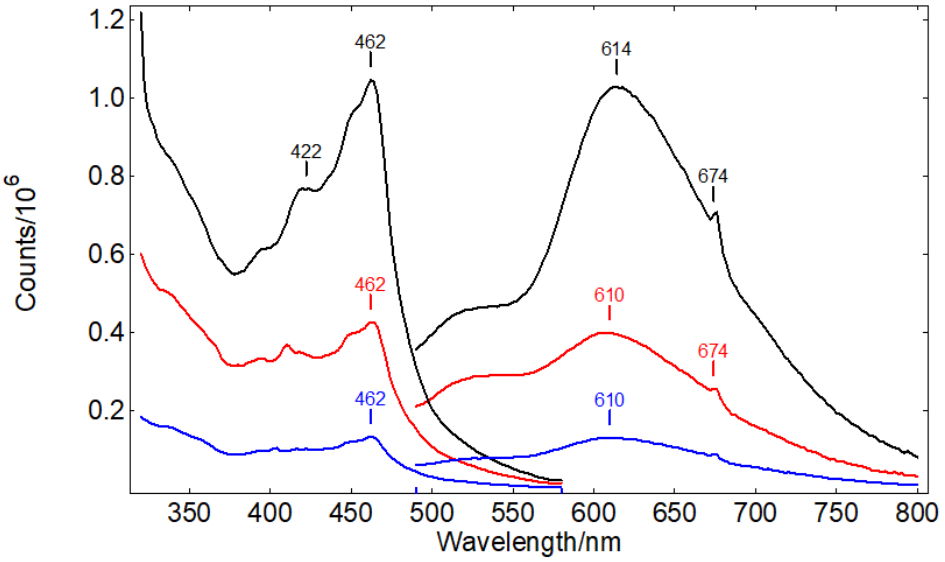

Figure 3.1 Overlay spectra of $[Ru(bpy)_3]^{2+}$ + TiO_2@Ag (black line), λ_{ex}=462 nm λ_{em}=614 nm, $[Ru(bpy)_3]^{2+}$ (red line) λ_{ex}=462 nm λ_{em}=610 nm, and $[Ru(bpy)_3]^{2+}$ + TiO_2 (blue line) λ_{ex}=462 nm λ_{em}=610 nm

Excitation-emission spectra of the single ruthenium complex, TiO_2 and ruthenium complex and TiO_2@Ag core-shell nanoparticles ruthenium complex combinations were recorded in PMMA in form of thin films. Thin films were prepared following above mentioned procedures and composite were casted on Mylar substrates by means of Spin Coating Technique. When excited at 460 nm the PMMA embedded $[Ru(bpy)_3]^{2+}$ complex excited a wideband emission at 622 nm. When exposed to 100% nitrogen (N_2) and oxygen (O_2) alternately, the emission intensity exhibited a drop with can be characterized by $I_0/I = 1.58$. Figure 3.2 I and II reveal the excitation emission and oxygen induced excitation emission characteristics of the sensing materials, respectively.

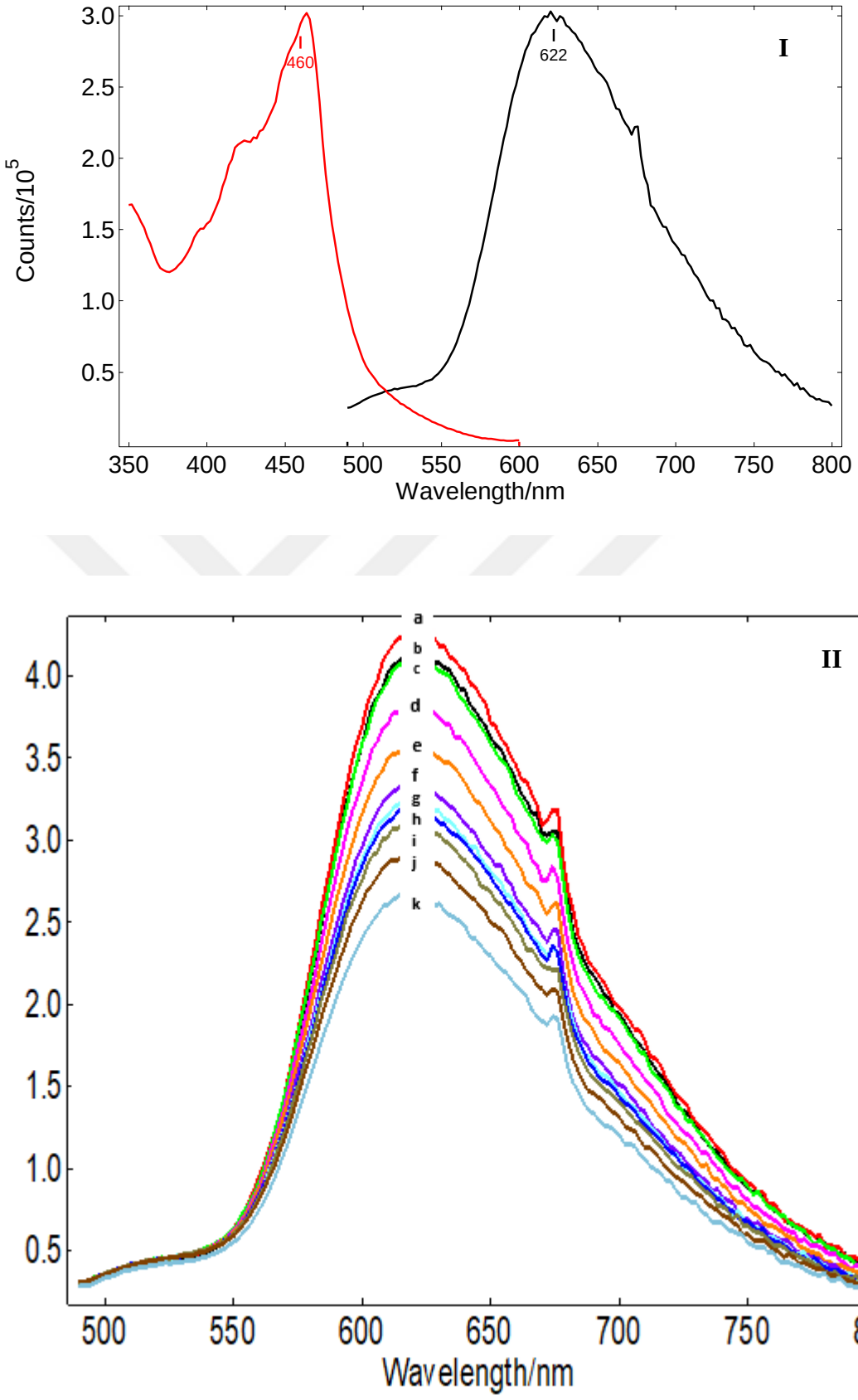

Figure 3.2 I: The excitation emission properties (λ_{ex}=460 nm λ_{em}=622 nm) of the $[Ru(bpy)_3]^{2+}$based sensing material, II: oxygen induced response of the sensing material. (slit width 10:10 nm, the oxygen concentration, O_2 %, a:0, b:10 c:20, d:30, e: 40, f: 50 g: 60 h: 70 i: 80 j: 90 k: 100)

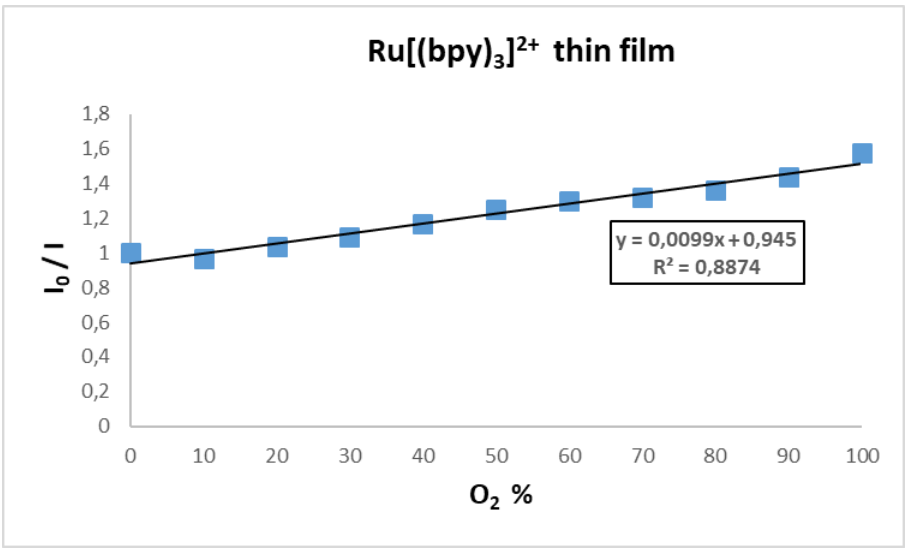

Figure 3.3 Stern-Volmer plot derived from quenching based data of $[Ru(bpy)_3]^{2+}$based sensing material

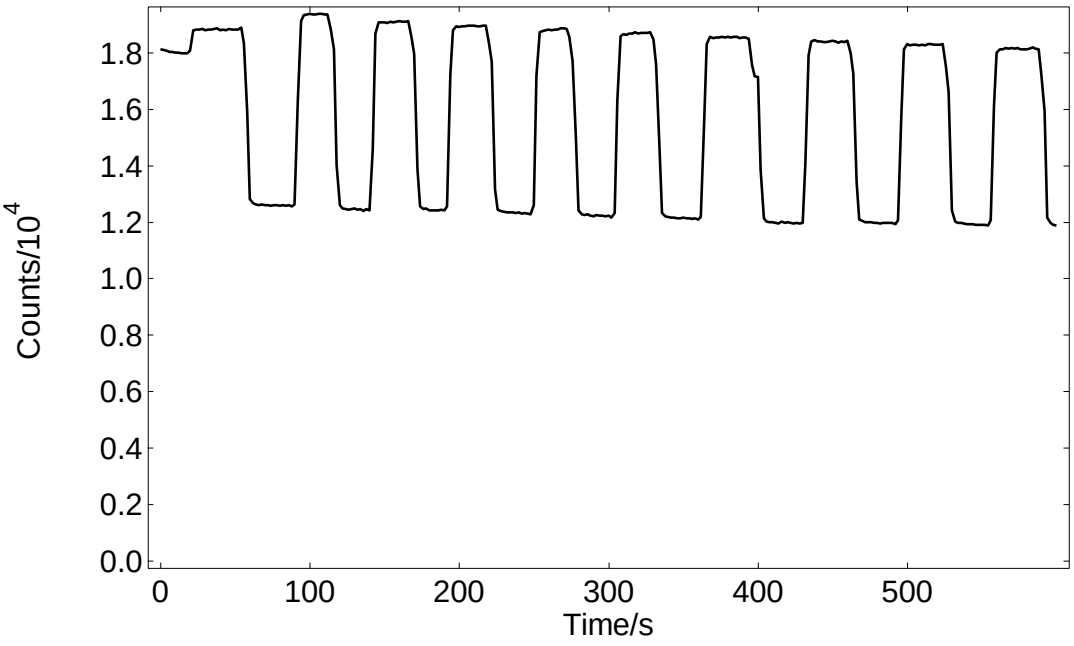

Figure 3.4 Kinetic results of the thin film of the $[Ru(bpy)_3]^{2+}$ in PMMA matrix. The upper and lower signals were acquired at deoxygenated and fully oxygenated conditions, respectively

Fig 3.3 and 3.4 reveal Stern-Volmer plot and oxygen induced kinetic response of the individual ruthenium complex in embedded form in PMMA.

Herein effect of the presence of the TiO_2@Ag core-shell structures on the spectral characteristics of the $[Ru(bpy)_3]^{2+}$ complex were investigated. Interestingly the excitation and emission maxima of the single ruthenium complex and ruthenium

complex+TiO_2@Ag core-shell structures exhibited the same behavior. However, oxygen induced response of the composite was better than that of the individual form. The I_0/I parameter was enhanced from 1.58 to 2.38 which is an indicator of higher sensitivity of the offered composite. Figure 3.5 I and II reveal excitation and emission and oxygen induced response characteristics of the core-shell containing forms, respectively.

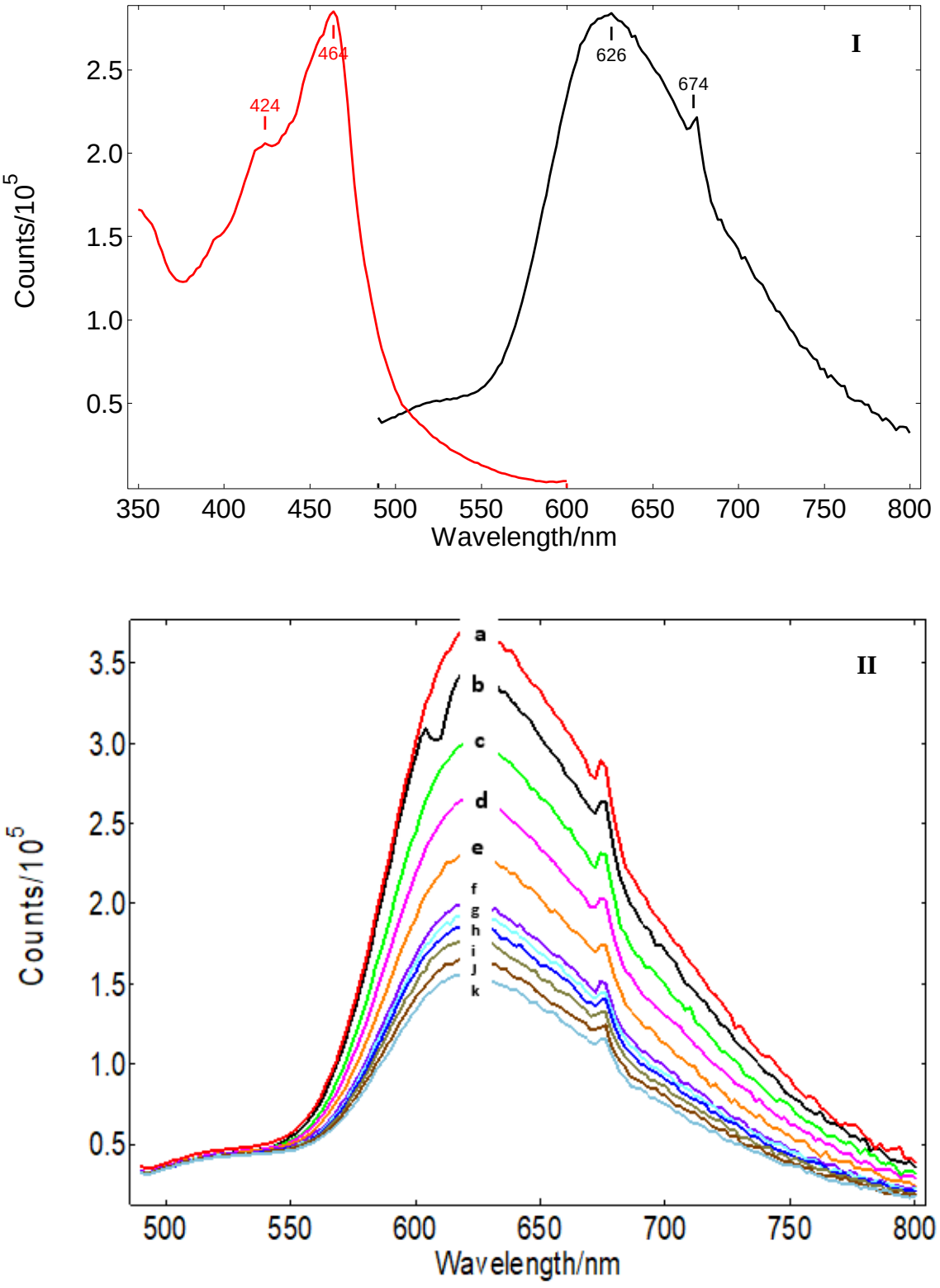

Figure 3.5 I: The excitation emission properties (λ_{ex}=464 nm λ_{em}=626 nm) of the $[Ru(bpy)_3]^{2+}$+TiO_2@Ag based composite material, II: oxygen induced response of the sensing material. (slit width 10:10 nm, the oxygen concentration, O_2 %, a:0, b:10 c:20, d:30, e: 40, f: 50 g: 60 h: 70 i: 80 j: 90 k: 100)

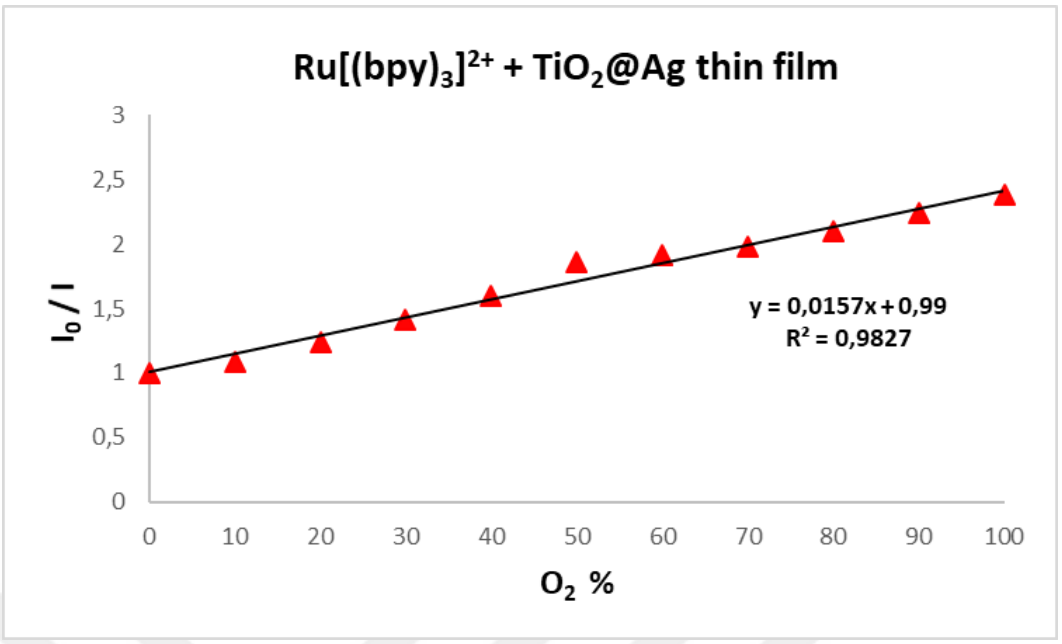

Figure 3.6 Stern-Volmer plot derived from quenching based data of the $[Ru(bpy)_3]^{2+}$+TiO_2@Ag nanoparticles containing PMMA based sensing thin film

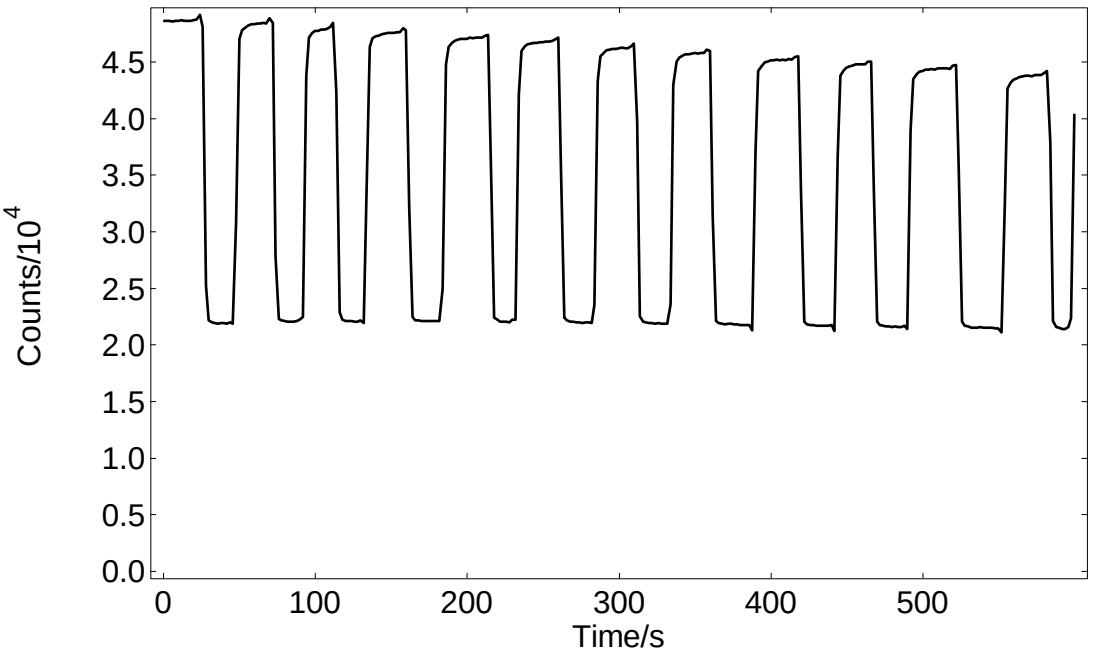

Figure 3.7 Kinetic results of the thin film of the $[Ru(bpy)_3]^{2+}$+TiO_2@Ag in PMMA matrix. The upper and lower signals were acquired at deoxygenated and fully oxygenated conditions, respectively

Figure 3.6 and 3.7 reveal Stern-Volmer Plot and oxygen induced kinetic response of the additive containing ruthenium complex in embedded form in PMMA. When the Stern-Volmer plots are compared to each other the enhancement both in the slope

and regression coefficient can easily be seen. While the nano-additive free composite exhibiting the calibration equation of y=0.0099x + 0.945, the nano-additive containing form yielded the plot of y=0.157x + 0.99 where the slope approximately 16 fold enhanced. Additionally, the regression coefficient developed from 0.8874 to 0.9827 which is an indicator of better linearity.

3.1.2 Lifetime Measurements

Figure 3.8 and 3.9 indicate decay curves of the additive-free and TiO_2@Ag core-shell containing organoruthenium complex based composites, respectively. Decay curves were acquired under excitation by a 460 nm diode laser. In both cases the composites excibited three exponentional decay behaviour with decay times of 153.74 and 203.46 ns. Presence of the TiO_2@Ag core-shell structures in the matrix along with ruthenium complex enhanced the overall decay time under ambient air. The enhancement in the long lifetime component was very distinct.

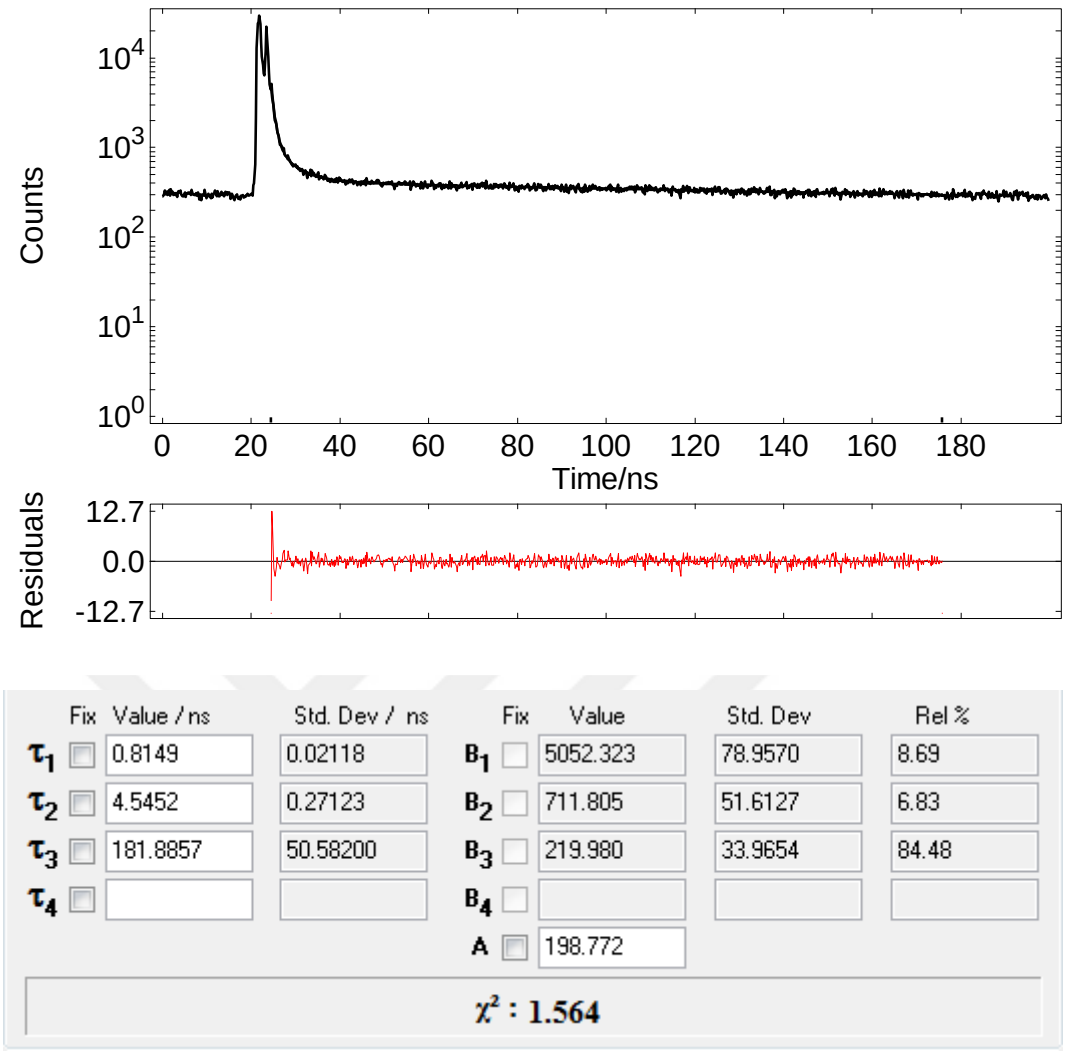

	Fix	Value / ns	Std. Dev / ns		Fix	Value	Std. Dev	Rel %
τ_1	☐	0.8149	0.02118	B_1	☐	5052.323	78.9570	8.69
τ_2	☐	4.5452	0.27123	B_2	☐	711.805	51.6127	6.83
τ_3	☐	181.8857	50.58200	B_3	☐	219.980	33.9654	84.48
τ_4	☐			B_4	☐			
				A	☐	198.772		

χ^2 : 1.564

Figure 3.8 Lifetime measurements of $[Ru(bpy)_3]^{2+}$ in PMMA matrix under ambient air

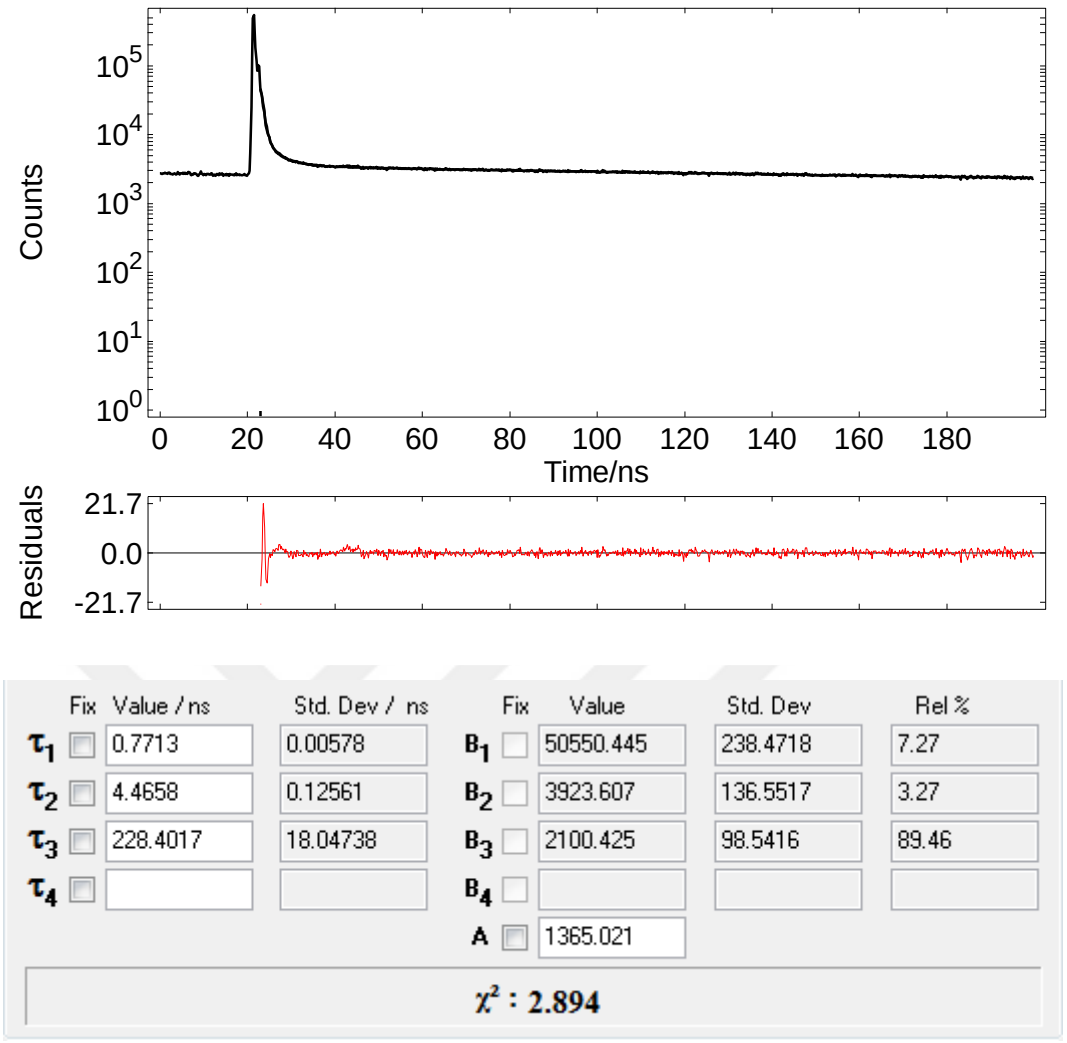

	Fix	Value / ns	Std. Dev / ns		Fix	Value	Std. Dev	Rel %
τ_1	☐	0.7713	0.00578	B_1	☐	50550.445	238.4718	7.27
τ_2	☐	4.4658	0.12561	B_2	☐	3923.607	136.5517	3.27
τ_3	☐	228.4017	18.04738	B_3	☐	2100.425	98.5416	89.46
τ_4	☐			B_4	☐			
				A	☐	1365.021		

χ^2 : 2.894

Figure 3.9 Lifetime measurements of $[Ru(bpy)_3]^{2+}$+TiO_2@Ag in PMMA matrix under ambient air

CHAPTER FOUR
CONCLUSION

In this work, the commercially available oxygen sensing $[Ru(bpy)_3]^{2+}$ complex was prepared in form of thin films in plasticized PMMA matrix along with TiO_2 and core-shell TiO_2@Ag nanoparticles.

The TiO_2 nanoparticles were synthesized via sol-gel technique. The core-shell structures were obtained with chemical reduction synthesis approach and characterized by X-ray diffraction spectrophotometer (XRD). The XRD spectra revealed 100% anatase phase of the TiO_2 nanoparticles. For the coated particles, the XRD spectra indicated the fully silver coated forms.

Oxygen induced sensitivity of the $[Ru(bpy)_3]^{2+}$ is prominent . On the other hand, the TiO_2 and or core-shell TiO_2@Ag structures have a potential to absorb and emit at broad band. Therefore we investigated the interactions between these two optically active structures. Presence of the TiO_2 resulting with a signal drop while presence of the core-shell structures within the composite resulted in signal enhancement of the $[Ru(bpy)_3]^{2+}$ based oxygen sensitive materials.

REFERENCES

Amao, Y. (2003). Probes and polymers for optical sensing of oxygen. *Microchimica Acta, 143*(1), 1–12.

Aydın, İ. (2017). *Investigation of nano-scale Sr4Al14O25: Eu2+/Dy3+ phosphors for optical chemical sensing purposes*. M.Sc Thesis, Dokuz Eylül University, İzmir.

Bancroft, H. R., Moore, C. A., & Frazier, J. L. (1976). Development of a biochemical profile for mass-reared boll weevils (Coleoptera: Curculionidae). *Comparative Biochemistry and Physiology Part C: Comparative Pharmacology*, *53*(1), 9-12.

Blasse, G., Grabmaier, B. C., Blasse, G., & Grabmaier, B. C. (1994). How does a luminescent material absorb its excitation energy? *Luminescent Materials, 203*, 10–32.

Borisov, S. M., & Vasil, V. V. (2004). New optical sensors for oxygen based on phosphorescent cationic water-soluble Pd (II), Pt (II), and Rh (III) Porphyrins. *Journal of Analytical Chemistry*, *59*(2), 155–159.

Bos, A. J. J. (2006). Theory of thermoluminescence. *Radiation Measurements*, *41*, 45-56.

Bruner, B., Walker, M. B., Ghimire, M. M., Zhang, D., Selke, M., Klausmeyer, K. K., … &Farmer, P. J. (2014). Ligand-based photooxidations of dithiomaltolato complexes of Ru(ii) and Zn(ii): Photolytic CH activation and evidence of singlet oxygen generation and quenching. *Dalton Transactions*, *43*(30), 11548–11556.

Choi, M. M. F., & Xiao, D. (1999). Linear calibration function of luminescence quenching-based optical sensor for trace oxygen analysis. *Analyst*, *124*(5), 695–698.

Chu, C. S., & Chuang, C. Y. (2014). Highly sensitive fiber-optic oxygen sensor based on palladium tetrakis (4-carboxyphenyl)porphyrin doped in ormosil. *Journal of Luminescence*, *154*, 475–478.

Chu, C. S., & Lo, Y. L. (2011). Highly sensitive and linear calibration optical fiber oxygen sensor based on Pt(II) complex embedded in sol-gel matrix. *Sensors and Actuators, B: Chemical*, *155*(1), 53–57.

Clark, L. C. (1956). Monitor and control of blood and tissue oxygen tensions. *Transactions American Society for Artificial Internal Organs*, *2*(1956), 41–48.

Cui, W., Liu, R., Manna, E., Park, J. M., Fungura, F., Shinar, J., & Shinar, R. (2015). Oxygen and relative humidity monitoring with films tailored for enhanced photoluminescence. *Analytica Chimica Acta*, *853*(1), 563–571.

de Acha, N., Elosúa, C., Martínez, D., Hernáez, M., Matías, I. R., & Arregui, F. J. (2017). Comparative study of polymeric matrices embedding oxygen-sensitive fluorophores by means of Layer-by-Layer nanosassembly. *Sensors and Actuators, B: Chemical*, *239*, 1124–1133.

Delice, T. K. (2018) *Investigation of corrosion properties of Ni matrix nanocomposite coatings produced by electrodeposition technique*. M.Sc Thesis, Dokuz Eylül University, İzmir.

Demas, J. N., DeGraff, B. A., & Coleman, P. B. (1999). Peer Reviewed: Oxygen Sensors Based on Luminescence Quenching. *Analytical Chemistry*, *71*(23), 793A-800A.

Elsayed, S. A., Gaml, E. A., & Nasher, M. A. (2018). New ruthenium (II) bipyridine complex bearing 2-aminophenylbenzimidazole: Synthesis, spectral characterization and optical properties. Optical Materials, 84, 8-15.

Franciscato, D. S., Matias, T. A., Shinohara, J., Gonçalves, J. M., Coelho, N. P., Fernandes, C. S., … de Souza, V. R. (2018). Thiosemicarbazone@Gold

nanoparticle hybrid as selective SERS substrate for Hg2+ions. *Spectrochimica Acta - Part A: Molecular and Biomolecular Spectroscopy*, *204*, 174–179.

Ghosh Chaudhuri, R., & Paria, S. (2012). Core/shell nanoparticles: Classes, properties, synthesis mechanisms, characterization, and applications. *Chemical Reviews*, *112*(4), 2373–2433.

Gryczynski, I., Malicka, J., Holder, E., DiCesare, N., & Lakowicz, J. R. (2003). Effects of metallic silver particles on the emission properties of [Ru(bpy)3]2+. *Chemical Physics Letters*, *372*(3–4), 409–414.

Gulino, A., Giuffrida, S., Mineo, P., Purrazzo, M., Scamporrino, E., Ventimiglia, G., … Fragalà, I. (2006). Photoluminescence of a covalent assembled porphyrin-based monolayer: Optical behavior in the presence of O2. *Journal of Physical Chemistry B*, *110*(33), 16781–16786.

Ishiji, T., & Kaneko, M. (1995). Photoluminescence of pyrenebutyric acid incorporated into silicone film as a technique in luminescent oxygen sensing. *The Analyst*, *120*(6), 1633–1638.

Jain, P. K., Huang, X., El-Sayed, I. H., & El-Sayed, M. A. (2009). ChemInform Abstract: Noble Metals on the Nanoscale: Optical and Photothermal Properties and Some Applications in Imaging, Sensing, Biology, and Medicine. *Chem Inform*, *40*(14), 7–9.

Jiang, Z., Yu, X., Zhai, S., & Hao, Y. (2017). Ratiometric Dissolved Oxygen Sensors Based on Ruthenium Complex Doped with Silver Nanoparticles. *Sensors*, *17*(3), 548.

Kandimalla, V. K. (2010). Influence of Metal Nanoparticles on Fluorescence Properties. M.Sc Thesis, Eastern Michigan University, Michigan.

Keskin, O. Y., Dalmis, R., Birlik, I., & Azem, N. F. A. (2020). Comparison of the effect of non-metal and rare-earth element doping on structural and optical

properties of CuO/TiO2 one-dimensional photonic crystals. *Journal of Alloys and Compounds*, *817*, 153262.

Khatami, M., Alijani, H. Q., & Sharifi, I. (2018). Biosynthesis of bimetallic and core-shell nanoparticles: Their biomedical applications - A review. *IET Nanobiotechnology*, *12*(7), 879–887.

Kurihara, R., Ikegami, R., Asahi, W., & Tanabe, K. (2018). Phosphorescent ruthenium complexes with bromopyrene unit that enhance oxygen sensitivity. *Bioorganic & Medicinal Chemistry*, *26*(16), 4595-4601.

Maia, P. J. S., de Aguiar, I., dos Santos Velloso, M., Zhang, D., dos Santos, E. R., de Oliveira, J. R., … Carlos, R. M. (2018). Singlet oxygen production by a polypyridine ruthenium (II) complex with a perylene monoimide derivative: A strategy for photodynamic inactivation of Candida albicans. *Journal of Photochemistry and Photobiology A: Chemistry*, *353*, 536–545.

Mao, Y., Mei, Z., Wen, J., Li, G., Tian, Y., Zhou, B., & Tian, Y. (2018). Honeycomb structured porous films from a platinum porphyrin-grafted poly(styrene-co-4-vinylpyridine) copolymer as an optical oxygen sensor. *Sensors and Actuators, B: Chemical*, *257*, 944–953.

Microtechnologies, S. (2005). New fabrication technologies. *American Ceramic Society Bulletin*, *84*(7), 79–134.

Miller, E. (2011). Fluorescence properties of a ruthenium complex in silane sols and gels at different pH. *Journal of Non-Crystalline Solids*, *357*(4), 1285–1290.

Mills, A. (1997). Optical oxygen sensors. *Platinum Metals Review*, *41*(3), 115–127.

Murthy, K. V. R., & Virk, H. S. (2014). Luminescence phenomena: An introduction. *Defect and Diffusion Forum*, *347*, 1–34.

Nomoev, A. V., Bardakhanov, S. P., Schreiber, M., Bazarova, D. G., Romanov, N. A., Baldanov, B. B., & Syzrantsev, V. V. (2015). Structure and mechanism of the formation of core-shell nanoparticles obtained through a one-step gas-phase synthesis by electron beam evaporation. *Beilstein Journal of Nanotechnology*, *6*(1), 874–880.

Ocakoglu, K., Okur, S., Aydin, H., & Emen, F. M. (2016). The effect of annealing temperature on the optical properties of a ruthenium complex thin film. *Thin Solid Films*, *612*, 225–230.

Ongun, M. Z., Oter, O., Sabanci, G., Ertekin, K., & Celik, E. (2013). Enhanced stability of ruthenium complex in ionic liquid doped electrospun fibers. *Sensors and Actuators, B: Chemical*, *183*, 11–19.

Raguse, J. M., & Sites, J. R. (2015). Correlation of Electroluminescence with Open-Circuit Voltage from Thin-Film CdTe Solar Cells. *IEEE Journal of Photovoltaics*, *5*(4), 1175–1178.

Papkovsky, D. B. (2004). Methods in optical oxygen sensing: protocols and critical analyses. *Methods in Enzymology 381*, 715-735.

Tian, Y., Shumway, B. R., Gao, W., Youngbull, C., Holl, M. R., Johnson, R. H., & Meldrum, D. R. (2010). Influence of matrices on oxygen sensing of three sensing films with chemically conjugated platinum porphyrin probes and preliminary application for monitoring of oxygen consumption of Escherichia coli (E. coli). *Sensors and Actuators, B: Chemical*, *150*(2), 579–587.

Toro, M. M. S., Fernandez-Sanchez, J. F., Baranoff, E., Nazeeruddin, M. K., Graetzel, M., & Fernandez-Gutierrez, A. (2010). Novel luminescent Ir(III) dyes for developing highly sensitive oxygen sensing films. *Talanta*, *82*(2), 620–626.

Vacher, M., Fdez. Galván, I., Ding, B. W., Schramm, S., Berraud-Pache, R., Naumov, P., ... & Baader, W. J. (2018). Chemi-and bioluminescence of cyclic peroxides. *Chemical Reviews*, *118*(15), 6927-6974.

Wang, X. D., & Wolfbeis, O. S. (2014). Optical methods for sensing and imaging oxygen: Materials, spectroscopies and applications. *Chemical Society Reviews*, *43*(10), 3666–3761.

Wang, X. D., Chen, H. X., Zhao, Y., Chen, X., & Wang, X. R. (2010). Optical oxygen sensors move towards colorimetric determination. *TrAC Trends in Analytical Chemistry*, *29*(4), 319-338.

White, T. A., Arachchige, S. M., Sedai, B., & Brewer, K. J. (2010). Emission spectroscopy as a probe into photoinduced intramolecular electron transfer in polyazine bridged Ru(II),Rh(III) supramolecular complexes. *Materials*, *3*(8), 4328–4354.

Wolfbeis, O. S. (2015). Luminescent sensing and imaging of oxygen: Fierce competition to the Clark electrode. *BioEssays*, *37*(8), 921–928.

Wu, S., Fan, Z., Wang, W., Fan, H., Mei, Z., Sun, D., … &Tian, Y. (2018). Microfabricable ratiometric gaseous oxygen sensors based on inorganic perovskite nanocrystals and PtTFPP. *Sensors and Actuators, B: Chemical*, *271*, 104–109.

Wu, W., Wu, W., Ji, S., Guo, H., Song, P., Han, K., … &Zhao, J. (2010). Tuning the emission properties of cyclometalated platinum(II) complexes by intramolecular electron-sink/arylethynylated ligands and its application for enhanced luminescent oxygen sensing. *Journal of Materials Chemistry*, *20*(43), 9775–9786.

Xu, W., Kneas, K. A., Demas, J. N., & DeGraff, B. A. (1996). Oxygen sensors based on luminescence quenching of metal complexes: Osmium complexes suitable for laser diode excitation. *Analytical Chemistry*, *68*(15), 2605–2609.

Xue, R., Behera, P., Xu, J., Viapiano, M. S., & Lannutti, J. J. (2014). Polydimethylsiloxane core-polycaprolactone shell nanofibers as biocompatible, real-time oxygen sensors. *Sensors and Actuators, B: Chemical*, *192*, 697–707.

Yamamoto, A. (2003). Synthesis, characterization and photoluminescence of ZrO2:Eu3+ nanocrystals. *Current Methods in Inorganic Chemistry*, *3*, 1–63.

Yoshihara, T., Hirakawa, Y., Hosaka, M., Nangaku, M., & Tobita, S. (2017). Oxygen imaging of living cells and tissues using luminescent molecular probes. *Journal of Photochemistry and Photobiology C: Photochemistry Reviews*, *30*, 71–95.

Zhang, H., Lei, B., Mai, W., & Liu, Y. (2011). Oxygen-sensing materials based on ruthenium(II) complex covalently assembled mesoporous MSU-3 silica. *Sensors and Actuators, B: Chemical*, *160*(1), 677–683.

Zink, J. I., & Chandra, B. P. (1982). Light emission during growth and destruction of crystals. Crystalloluminescence and triboluminescence. *Journal of Physical Chemistry*, *86*(1), 5–7.